CHAPTER 4

EXPERIMENTATION ON MINICHANNEL HEAT SINK

4.1 Experimental setup and procedure

The layout and photograph of the experimental setup are illustrated in Fig. 4.1 and Fig. 4.2, respectively. Four main units exist in the system; flow loop, cooling, heating and measuring units. The flow loop consists of pipes, a test section, a flow meter and a pump. An in-built positive displacement pump attached to the constant temperature bath with an inverter, which is suitable for particulate flows, has been used. The test setup can be assembled and disassembled easily. The flow rate can be adjusted in the range of 6–30 lph. The flow rates are measured using a variable area flowmeter with a measuring range of 0-60 lph. A water bath circulator has been used just before the test section so that the working fluid can enter the test section at the inlet conditions. The test section includes a heater with AC supply, top and bottom plates, thermocouples, and acrylic plate materials. The acrylic plate is used as an insulator to cover the heat sink from the top. K-type thermocouples are inserted for temperature measurement. A differential pressure transducer is used to measure the pressure drop between the inlet and outlet of the heat sink. Three cartridge heaters (having each power of 150 W) located to the bottom of the heat sink. Constant and uniform heat fluxes are supplied to the channel from the bottom side. The cartridge heaters are connected to a variac transformer, and a range of constant heat flux of 8.3-66.67 W/cm^2 is applied to the bottom surface of the channel. NI data acquisition system (DAS) is used to extract the data from the system.

The experiments are conducted by using all the working fluids (DI water, nanofluids and hybrid nanofluids). After completion set of experiments using a hybrid

nanofluid, the supply of DI water is provided to the cleaning of the piping system to perform the experiments using different working fluid. The fluid has been taken from the supply reservoir into the system at three different inlet temperatures of 20°C, 30°C and 40°C through the pump, and the heat flux has been supplied to the system after the maximum Reynolds number (which remain constant) has been reached. Five K-type thermocouples are inserted at various locations to the bottom of the sink to measure average wall temperature. These K-type thermocouples have been calibrated before using in the present experimental research. During this process, wall temperature (T_s) and outlet temperature (T_{out}) both increases, but the constant inlet temperature (T_{in}) of hybrid nanofluid is ensured by the use of a temperature-controlled bath. Also, the thermal boundary layer grows at a particular section of the channel during this process. But after 40-45 min, steady-state condition achieved (i.e., thermal equilibrium condition) and the negligible fluctuation in wall temperature and outlet temperature has been observed (~0.0002°C/hour). The growth of the thermal boundary layer also does not occur. Thus, we assumed that there is no fluctuation in temperatures. So, we have done all the calculations on tested value. All the readings are measured using a combination of computer and NI data acquisition system. After data recording for a particular set, mass flow rate change to the next level and experiment is accomplished. The same experiments have been performed after 10 days and no significant changes have been observed in the readings. Also, all the experiments have been performed three times for each data set and the average of the three values is taken for the calculations.

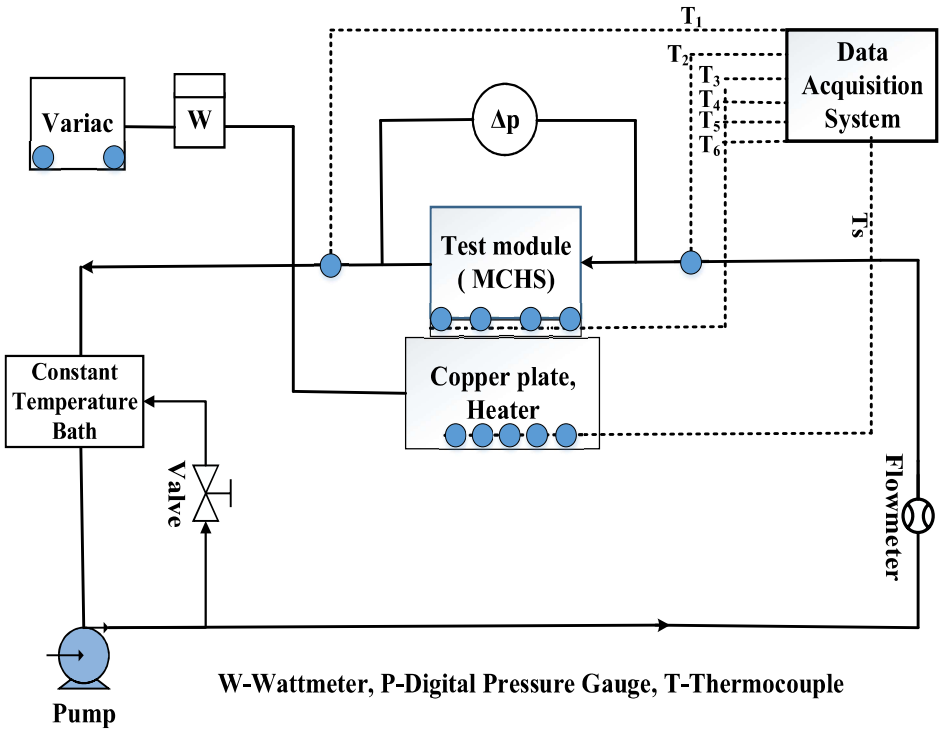

Fig. 4.1 Layout of experimental work

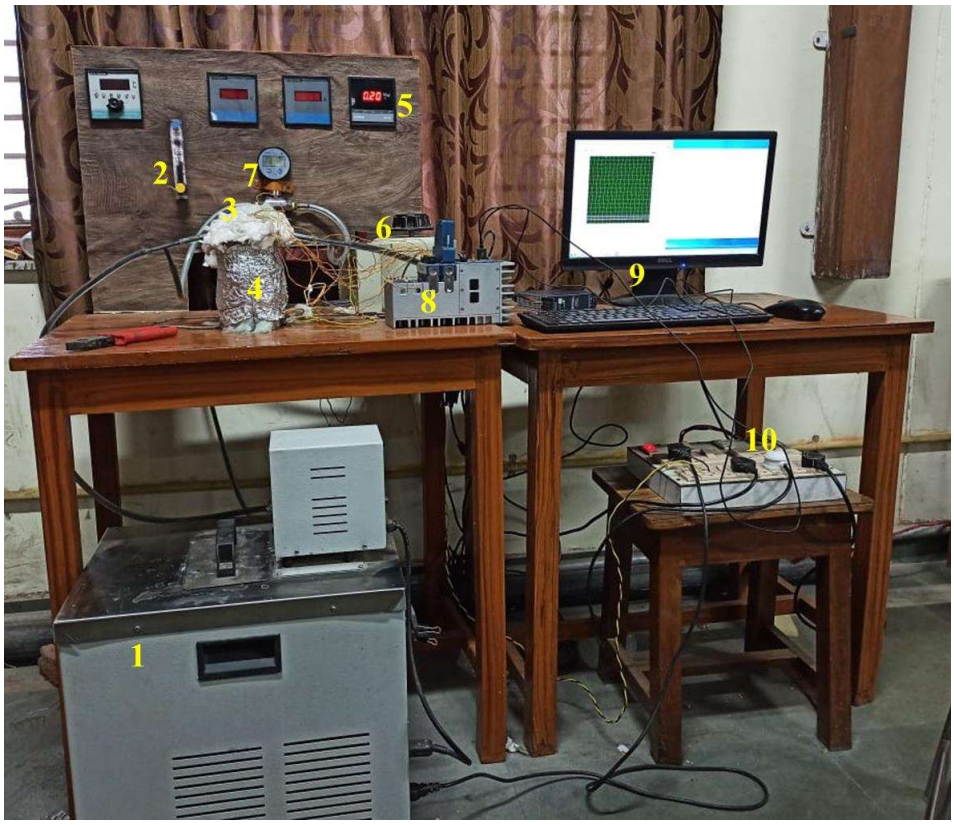

Fig. 4.2 Photograph of experimental Setup (1. Constant temperature bath, 2. Flowmeter, 3. Test module, 4. Heater, 5. Wattmeter, 6. Variac, 7. Pressure transducer, 8. NI DAQ module, 9. Computer monitor, 10. Power supply)

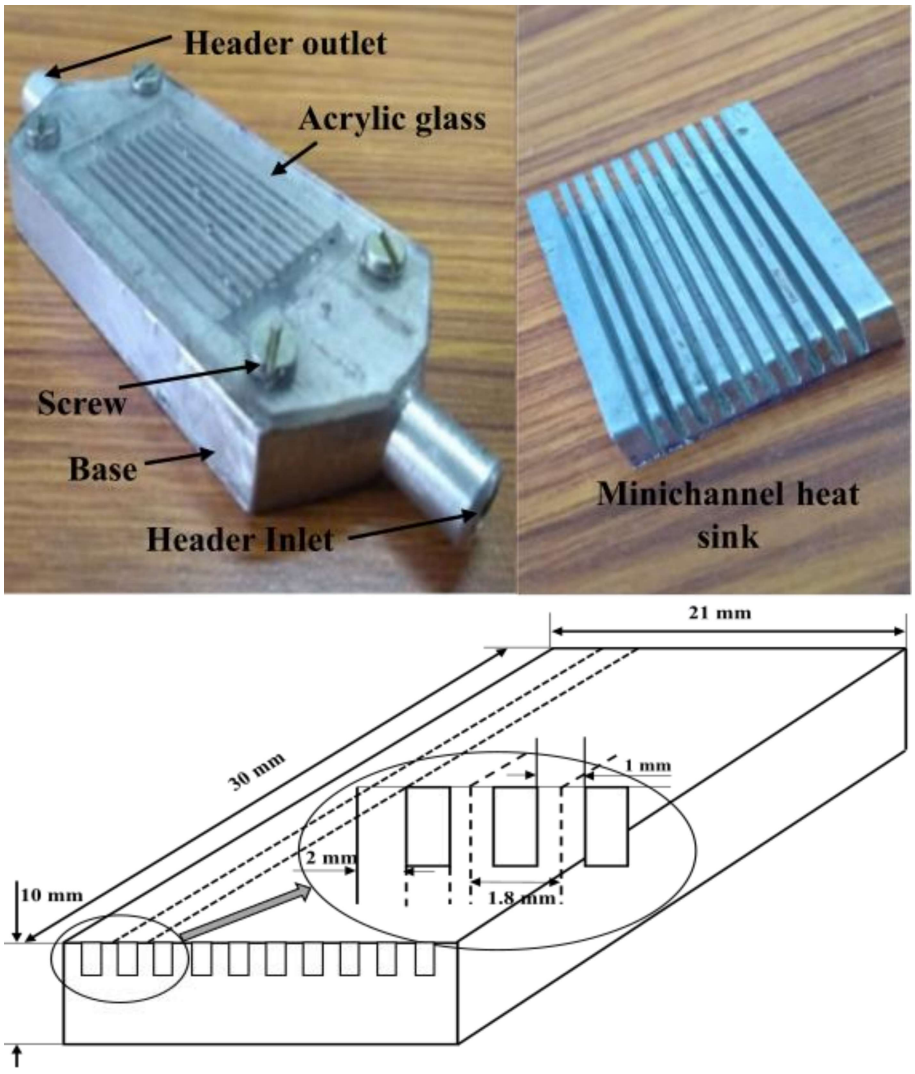

Fig. 4.3 Minichannel heat sink with schematics

4.2 Hydrothermal modelling

By using the volumetric flow rate, inlet and outlet temperatures, measured from the experiment, the heat transfer rate is obtained by,

$$\dot{Q} = \dot{V}\rho c_p (T_{out} - T_{in}) \tag{4.1}$$

In the case of phase change material (PCM) dispersed nanofluids, the heat transfer rate is obtained as (if $T_{in} < T_{f,PCM} < T_{out}$),

$$\dot{Q} = \dot{V}[(\rho c_p)_s (T_{f,PCM} - T_{in}) + \phi_{PCM}\rho_{PCM,s}\,\mathrm{L} + (\rho c_p)_l (T_{out} - T_{f,PCM})] \tag{4.2a}$$

$(\rho c_p)_s$ and $(\rho c_p)_l$ are volumetric heat capacities of nanofluid, when PCM in the solid phase and in the liquid phase, respectively. But as the fraction of PCM is very less, we have assumed no significant variation in density and specific heat of nanofluid when PCM is in solid-state and nanofluid when PCM liquid-state. L is the latent heat of fusion of PCM. Thus, Eq. (4.2a) is reduced to,

$$\dot{Q} = \dot{V}\rho c_p (T_{out} - T_{in}) + \varphi_{PCM}\dot{V}\rho_{PCM,s}\,\mathrm{L} \tag{4.2b}$$

Convective heat transfer coefficient is calculated by,

$$h = \frac{\dot{Q}}{A(T_s - T_m)} \tag{4.3}$$

Where, mean temperature of the fluid (T_m) is the average of inlet and exit temperatures. Average surface temperature (T_s) is measured by mean of five thermocouples reading, inserted at different locations to the bottom of the heat sink.

The effective heat transfer area (A) is calculated as,

$$A = N(w_{ch} + 2\eta_{fin}h_{ch})L_{ch} \tag{4.4}$$

Where, N is the number of channels, η_{fin} is fin efficiency, L_{ch}, w_{ch} and h_{ch} are length, width and height of the channel, respectively. Fin efficiency can be found out using Eq. 4.5 and Eq. 4.6 by iteration **(Ho and Chen, 2013)**, which are given by,

$$\eta_{fin} = \frac{\tanh(mh_{ch})}{mh_{ch}} \tag{4.5}$$

$$m = \sqrt{2h / (k_m w_{fin})} \tag{4.6}$$

Thermal resistance is estimated by,

$$R_{th} = \frac{T_s - T_m}{\dot{Q}} \tag{4.7}$$

The hydraulic diameter of minichannel is defined as,

$$d_h = \frac{2w_{ch}h_{ch}}{w_{ch} + h_{ch}} \tag{4.8}$$

Heat transfer effectiveness is given by **(Ho et al., 2019)**,

$$\varepsilon = \frac{h_{nf}}{h_{bf}} \tag{4.9}$$

The Nusselt number (Nu) is given as,

$$Nu = \frac{hd_h}{k} \tag{4.10}$$

u_m is mean or average fluid velocity and it is estimated based on volumetric flow rate, it is defined as

$$u_m = \frac{\dot{V}}{Nw_{ch}h_{ch}} \tag{4.11}$$

The Reynolds number is given by,

$$\mathrm{Re} = \frac{\rho u_m d_h}{\mu} \tag{4.12}$$

Thermal effectiveness is given by [**Ho et al., 2014**],

$$\varepsilon_{th} = 1 - \frac{(T_{s,\max} - T_{in})_{nf}}{(T_{s,\max} - T_{in})_{bf}} \tag{4.13}$$

The equation is adopted to calculate pressure drop in minichannel,

$$\Delta p = \Delta p_{\mathrm{Exp.}} - \rho g(Loss_{\mathrm{minor}}) \tag{4.14}$$

$Loss_{\text{minor}}$ = enlargement losses + contraction losses (4.15)

The schematic of minichannel heat sink with headers has been shown in Fig. 4.3. Schematic has been divided into different sections (1-5). Based on this, enlargement and contraction losses **(Cengel and Cimbala, 2006)** can be calculated by Eq. 4.16 to find out the total minor losses.

$$Loss_{\text{minor}} = \frac{u_1^2}{2g}\left(1-\left(\frac{A_1}{A_2}\right)\right)^2 + K_1.\frac{u_3^2}{2g} + \frac{u_3^2}{2g}\left(1-\left(\frac{N.A_3}{A_4}\right)\right)^2 + K_2.\frac{u_5^2}{2g} \quad (4.16)$$

Here, A_1=A_5 and A_2=A_4, $u_1 = \dot{V} / A_1$, $u_3 = \dot{V} / (NA_3)$, $A_3 = w_{ch}h_{ch}$ and $u_5 = \dot{V} / A_5$

Where, N is the number of channels, A_1, A_2, A_3, A_4 and A_5 are the areas in sections 1, 2, 3, 4 and 5, respectively. K_1 depends upon A_3/A_2 ratio and K_2 depends upon A_5/A_4 ratio. The friction factor is calculated by,

$$f = \frac{2d_h\Delta p}{L_{ch}\rho u_m^2} \quad (4.17)$$

Pumping power is calculated (based on pressure drop between outlet and inlet of heat sink) given by,

$$P_P = \dot{V} \times \Delta p \quad (4.18)$$

The combined effect of heat transfer coefficient and pressure drop due to the application of nanoparticles is studied through the comparison factor, J, which is a ratio of heat transfer coefficient to pressure drop **(Bhattad and Sarkar, 2021**). It is given by,

$$J = \frac{h}{\Delta p}$$

The cooling effect per unit pumping power (COP) is estimated by **(Ho et al., 2019)**,

$$COP = \frac{\dot{Q}}{P_P} \quad (4.19)$$

Thermal effectiveness (ε_{th}) given in Eq. 4.13 and COP provided in Eq. 4.19 are two different parameters. Thermal effectiveness is a heat transfer parameter where only temperatures matter. The maximum value of Thermal effectiveness can be 1 (ideal condition). This parameter is used to assess the usefulness of using water-based hybrid nanofluids for thermal management by comparing the maximum wall temperature of the heat sink to that of using pure water. While COP is the hydrothermal parameter in which both heat transfer and pumping power are considered. It deals with the rate of heat transfer if unit pumping power is consumed.

The figure of merit (FOM) is given by **(Ho et al., 2019)**,

$$FOM = \frac{\varepsilon}{(P_{p,nf} / P_{p,bf})^{1/3}} \tag{4.20}$$

Performance evaluation criteria (PEC) is calculated as,

$$PEC = \frac{Nu_{nf} / Nu_{bf}}{(f_{nf} / f_{bf})^{1/3}} \tag{4.21}$$

Consider the heat sink as a thermal system. There is irreversible loss due to temperature difference and pressure drop. Total entropy generation rate is calculated by applying entropy balance in control volume of the system **(Cheng et al., 2018)**,

$$S_{in} + dS_{gen} + \left(\frac{d\dot{Q}}{T_s}\right) = S_{out} \tag{4.22a}$$

Where, S_{in}, S_{out}, T_s, S_{gen} are the entropy inlet, entropy outlet, surface temperature and entropy generation in the system, respectively.

$$dS_{gen} = (S_{out} - S_{in}) - \left(\frac{d\dot{Q}}{T_s}\right) \tag{4.22b}$$

$$d\dot{Q} = \dot{m} c_p dT \tag{4.23}$$

By considering the working fluid as incompressible fluid (i.e., the density of working fluid constant) and all other properties constant throughout the process. Eq. (4.22b) is converted for a control volume and given as,

$$\dot{S}_{out} - \dot{S}_{in} = \int \dot{m}\left(c_p \frac{dT}{T} - \frac{dp}{\rho T} \right) = \int d\dot{S}_{gen} + \int \frac{\delta \dot{Q}}{T_s} \tag{4.24}$$

In Eq. 4.24, T_s is the surface temperature of the heat sink, which is measured by thermocouples and after steady-state condition so, T_s is assumed as constant. By Integration Eq. 4.24 between inlet and outlet of the heat sink, total entropy generation rate of fluid inside the heat sink is given by,

$$S_{gen} = \dot{m}\left(c_p \ln\left(\frac{T_{out}}{T_{in}} \right) - \frac{(p_{out} - p_{in})}{\rho T_m} \right) - \left(\frac{\dot{m} c_p (T_{out} - T_{in})}{T_s} \right) \tag{4.25}$$

$$S_{gen} = \dot{m}\left(c_p \ln\left(\frac{T_{out}}{T_{in}} \right) + \frac{\Delta p}{\rho T_m} \right) - \left(\frac{\dot{Q}}{T_s} \right) \tag{4.26}$$

Where, T_m is the mean temperature and it is given by $T_m = (T_{in} + T_{out})/2$.

There are six variables with their range and mean value has been tabulated in **Table 4.1**. The variables are fluid inlet temperature, volume flow rate, volume concentration of nanoparticles, mixing ratio, heat flux and channel aspect ratio. The effect of these variables on the performance of minichannel heat sink is investigated.

Table 4.1 Variables with their range and mean value

Variables	**Range**	**Mean**
Inlet temperature (T_{in})	20-40^{o}C	30^{o}C
Volume flow rate	0.1-0.5 lpm	0.3 lpm
Volume concentration (ϕ)	0.01 and 0.1%	-
Mixing ratio (ϕ_1/ϕ_2)	5:0 to 0:5	2.5:2.5

Heat flux (Q)	33.33 -66.68 W/cm^2	50 W/cm^2
Aspect ratio (AR), (h_{ch}/w_{ch})	2.5, 3.75, 5	3.75

4.3 Uncertainty analysis and validation

In the equation, R is a function of independent variables X_1, X_2, X_3……X_n, and W_1, W_2, W_3……,W_n are uncertainties of independent variables. Dimension, temperature, volume flow rate, pressure drop and heating power have been measured by appropriate instruments as Vernier caliper, thermocouple, rotameter, pressure transducer and wattmeter, having uncertainties of ± 0.02mm, ± 0.1°C, ± 0.5%, ± 0.25% and ± 0.25%, respectively. Uncertainty of dependent variables as convective heat transfer coefficient, friction factor, etc. is W. Uncertainty analysis of the convection heat transfer coefficient, Reynolds number, Nusselt number, friction factor, etc. have been performed by Eq. 4.27 given below **(Kline and McClintock, 1953)**. The values of uncertainty (W) obtained are given in **Table 4.2**.

$$W = \pm\left[\left(\frac{\partial R}{\partial X_1}W_1\right)^2 + \left(\frac{\partial R}{\partial X_2}W_2\right)^2 + \ldots\ldots\ldots\ldots\left(\frac{\partial R}{\partial X_n}W_n\right)^2\right]^{1/2} \quad (4.27)$$

Table 4.2 The uncertainties during the measurements of the experimental parameters

Variable	**Uncertainty value (%)**
T_{out}-T_{in} (K)	±0.07
T_s-T_m (K)	±0.09
Heat transfer rate, $\dot{Q}$ (W)	±2.87
Effective area, A (m^2)	±1.2
Hydraulic diameter, d_h (m)	±1.02

Volume flow rate, $\dot{V}$ (lpm)	±0.5
Velocity, u_m (m/s)	±0.78
Pressure drop, Δp (Pa)	±0.25
Thermal conductivity, k (W/m.K)	±2.0
Viscosity, μ (Pa/s)	±2.0
Density, ρ (Kg/m^3)	±2.0
Specific heat, c_p (J/Kg.K)	±2.0
Convective heat transfer coefficient, h (W/m^2.K)	±3.1
Friction factor, f	±2.76
Nusselt number, Nu	±3.83
Reynolds number, Re	±3.1
Comparison factor, h/Δp (m/s.K)	±3.12
FOM	±4.39
PEC	±5.57
COP	±2.92
Total entropy generation rate, S_{gen} (W/K)	±5.05

The experimental data of the friction factor obtained for Al_2O_3/DI water nanofluid is compared with the existing correlation available in the literature. Fig. 4.4 presents the comparison of experimental Nusselt number with available correlations in the literature. From the figure, it can be seen that the experimental Nusselt number is best suited to the Hausen correlation **(Sakanova et al., 2014)** developed for the thermal developing region but have some variation because of dissimilar heat flux condition. The validation of the experimental friction factor with available correlations in literature is shown in Fig. 4.5. Experimental friction factor value while considering minor losses (enlargement

losses and contraction losses) has good agreement with most of the existing correlations after Re=200. To calculate the pressure drop in minichannel, pressure losses in headers have to be subtracted from the experimental data using Eq. 4.16. The experimental friction factor is best matched with the correlation developed by **Jiang et al., 2001**.

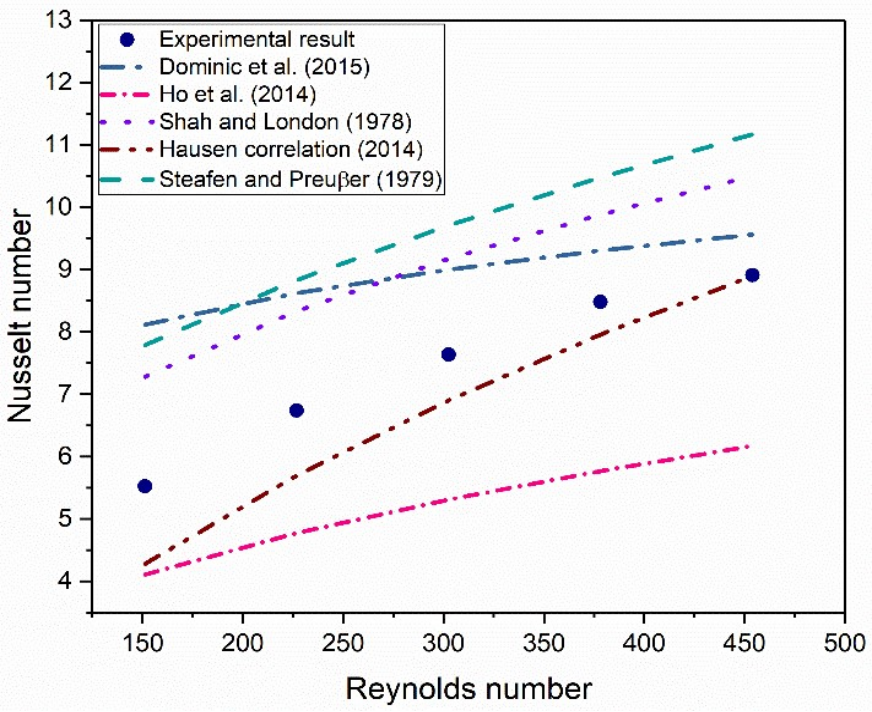

Fig. 4.4 Validation of experimental Nusselt number with available correlations

4.4 Results and discussion

The results of different parameters such as heat transfer characteristics (heat transfer coefficient, Nusselt number and thermal effectiveness), pressure drop characteristics (pressure drop and friction factor) and relative effect on heat transfer and fluid flow characteristics have been examined for considered working fluids. Effect on the figure of merit, performance evaluation criteria, coefficient of performance and total entropy generation for different hybrid nanofluids is also discussed in this study. The performance of minichannel heat sink is compared by different combinations of nanoparticles (oxide-PCM, oxide-oxide, oxide carbide, oxide-nitride, oxide-metal,

oxide-allotropes of carbons). Capric acid is taken as phase change materials. Different oxides (MgO, CuO, TiO_2), nitride (AlN), carbide (SiC), metal (Cu), allotropes of carbon (MWCNT and graphene) are considered in the present experimental study.

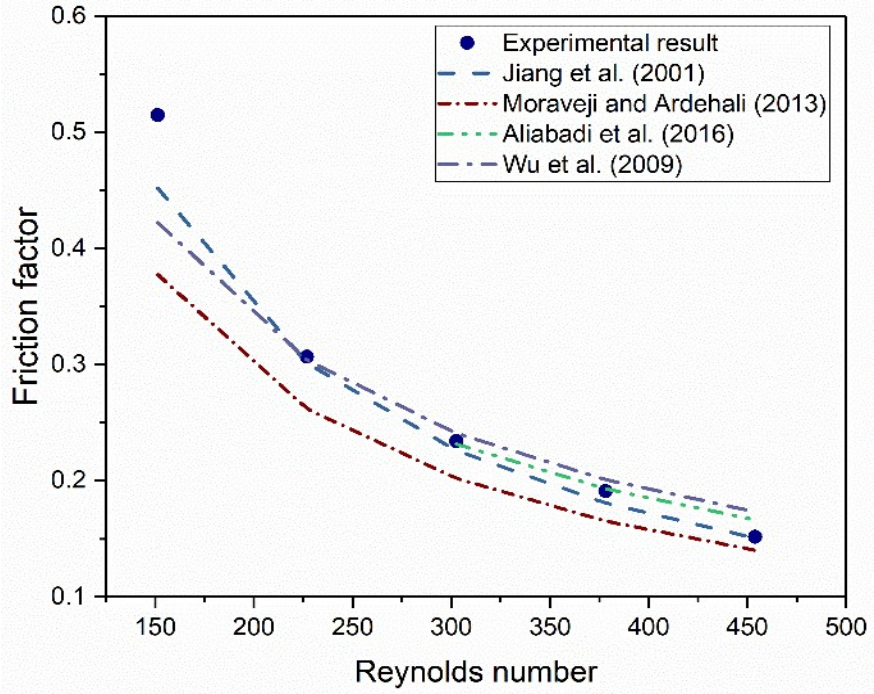

Fig. 4.5 Validation of experimental friction factor with available correlations

Different parameters for various working fluids at mean condition (T_{in}=30°C, ϕ=0.01 vol%, $\dot{V}$=0.3 lpm, mixing ratio=2.5:2.5, heat flux=50 W/cm^2, channel aspect ratio=3.75) are tabulated in **Table 4.3**. It can be concluded from Table 4.3, CNT dispersed nanofluid has the highest heat transfer coefficient but also has the highest penalty of pressure drop. Also, it shows the maximum entropy generation rate. It is analyzed that Al_2O_3+AlN mixture dispersed hybrid nanofluid yields best combined hydrothermal performance parameters such as comparison factor (h/Δp), FOM, PEC and COP.

Table 4.3 Different parameters at mean conditions (T_{in}=30°C, ϕ=0.01 vol%, $\dot{V}$ =0.3 lpm, mixing ratio=2.5:2.5, heat flux=50 W/cm^2, aspect ratio=3.75)

Nano-fluids	**Parameters**									
	h (W/m^{2}K)	**Nu**	**ε_{th}**	**Δp (Pa)**	**f**	**J (m/sK)**	**FOM**	**PEC**	**COP**	**S_{gen} (W/K)**
DI water	3258.2	6.62	-	125.61	0.24	25.94	-	-	166014.7	0.020147
Al_2O_3	3384.4	6.86	0.0050	138.64	0.27	24.41	1.00	1.00	155127.7	0.020526
TiO_2	3316.0	6.72	0.0028	138.64	0.27	23.92	0.99	0.98	152718	0.020303
CNT	4480.5	8.88	0.0476	207.11	0.40	21.63	1.16	1.13	126553.2	0.023105
PCM	3261.8	6.80	0.0208	150.00	0.29	21.74	0.94	0.97	136223.1	0.019112
Al_2O_3+TiO_2	3348.6	6.78	0.0039	138.63	0.27	24.15	0.99	0.99	153862.6	0.020408
Al_2O_3+CNT	4358.3	8.69	0.0421	162.52	0.31	26.82	1.23	1.20	158454.6	0.022922
Al_2O_3+PCM	3613.9	7.42	0.0509	145.53	0.28	24.83	1.06	1.07	149098.9	0.019563

Al_2O_3+MgO	3538.4	7.14	0.0134	134.01	0.26	26.40	1.06	1.06	165388.7	0.020881
Al_2O_3+CuO	3379.0	6.90	0.0037	139.66	0.27	24.20	1.01	1.00	154002.8	0.020557
Al_2O_3+SiC	3689.3	7.41	0.0218	128.35	0.25	28.74	1.13	1.11	177587.7	0.021188
Al_2O_3+AlN	4110.5	8.30	0.0338	129.90	0.25	31.64	1.25	1.24	190259.6	0.022369
Al_2O_3+Graphene	4445.7	8.98	0.0463	207.02	0.40	21.47	1.16	1.15	125891	0.023042
Al_2O_3+Cu	4227.3	8.48	0.0380	154.99	0.30	27.28	1.21	1.19	162817	0.022624

4.4.1 Comparison of various hybrid nanofluids

In Fig. 4.6, the heat transfer coefficient increases with the flow rate. The heat transfer coefficient increases with add on nanoparticles in the base fluid. This may be due to the increase in thermal conductivity, slip mechanisms, micro convection, nano-porous and nano-fin effects **(Tiwari et al., 2015)**. Allotropes of carbons (graphene nanoplates and MWCNT) dispersed hybrid nanofluids show maximum heat transfer coefficient. The maximum heat transfer coefficient is yielded by Al_2O_3+graphene/DI water hybrid nanofluid having value 5324.82 W/m^2.K. The maximum improvement is observed 43.12% and 37.74% for Al_2O_3+graphene/DI water hybrid nanofluid compared to DI water and Al_2O_3 nanofluid at 0.4 lpm, respectively. This is mainly ascribed to the very high thermal conductivity of graphene compared to all other nanoparticles. Another reason may be a higher specific surface area due to the higher aspect ratio of graphene nanoplates.

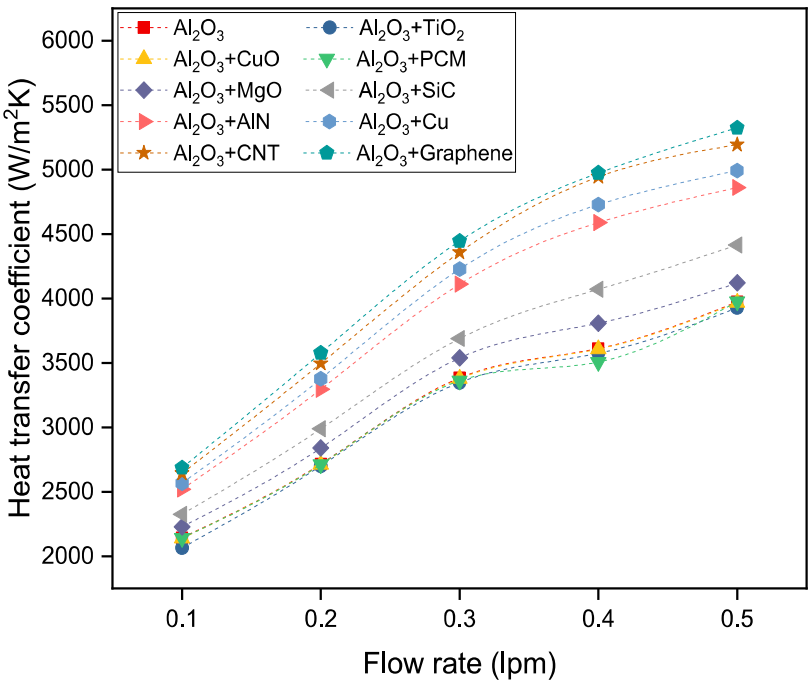

Fig. 4.6 Variation of heat transfer coefficient with flow rate

For a specific heat sink, heat transfer due to conduction is constant because it depends on the material properties, heat sink dimensions and heat source. But heat transfer due to convection strongly depends upon the fluid and flow properties. The variation of Nusselt number with Reynolds number for different working fluids is shown in Fig. 4.7. It states that the Nusselt number increases as the Reynold number increases. The nanoparticle's dispersion in the base fluid augments the Nusselt number. The calculated Nusselt number has a maximum value of about 10.75 observed for Al_2O_3+graphene based hybrid nanofluid. A maximum enhancement of 42.2% revealed for Al_2O_3+graphene mixture based hybrid nanofluid over base fluid at Re=337.84. As the Reynolds number is proportional to inlet velocity, the higher Reynold number means higher velocity. Movement and Inter-collision of nanoparticles, which enhances the heat transfer rate, is increased with inlet velocity (Reynold number) is the main cause for enhancement of Nusselt Number.

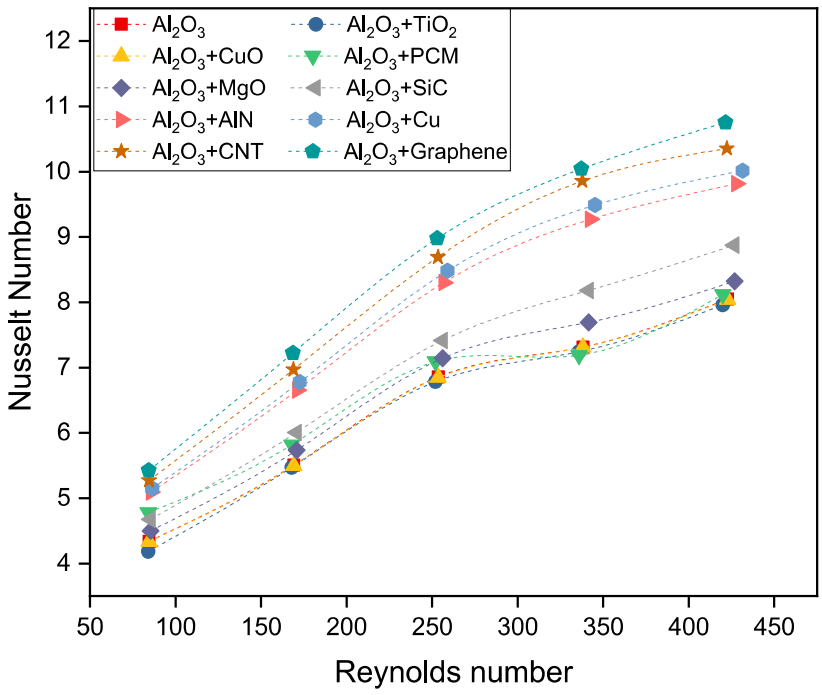

Fig. 4.7 Nusselt number with Reynolds number for different working fluids

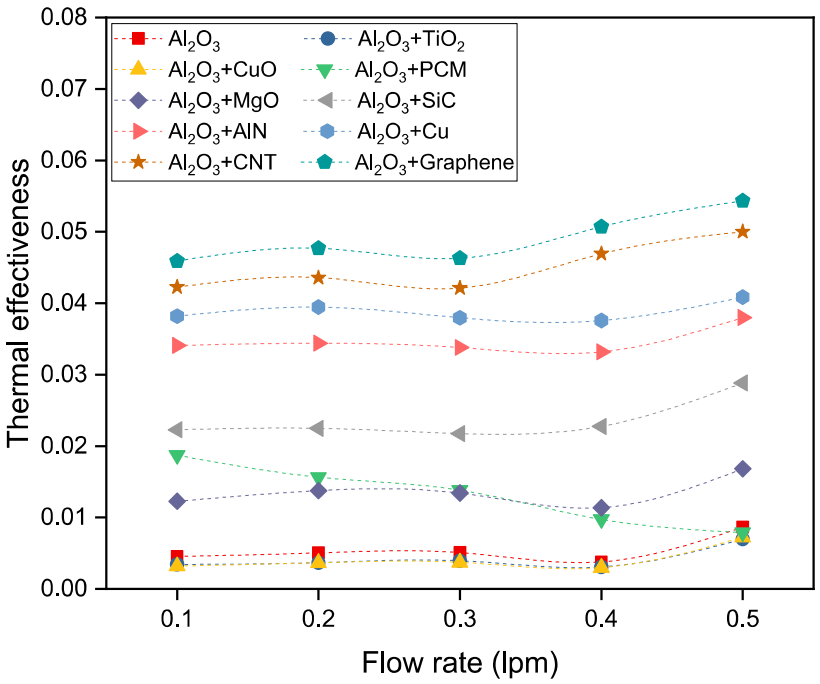

Fig. 4.8 Changing in thermal effectiveness with flow rate for different working fluids

The overall cooling performance of the system has been understood by the term thermal effectiveness. The thermal effectiveness of the system with the flow rate and for different coolants is shown in Fig. 4.8. It can be observed from the figure that high conductivity particles based nanofluids show high thermal effectiveness. It is because of these nanofluids extract more heat from the system as compared to low conductivity particles based nanofluids. Maximum thermal effectiveness is observed for the allotropes of carbon (CNT and graphene) dispersed hybrid nanofluid. Al_2O_3+CuO/DI water hybrid nanofluid shows the minimum thermal effectiveness. That conclude that this is not beneficial to use it for cooling purpose. First, the thermal effectiveness increases then decreases and again increases except Al_2O_3+PCM based nanofluids. Thermal effectiveness decreases with flow rate for Al_2O_3+PCM based nanofluids.

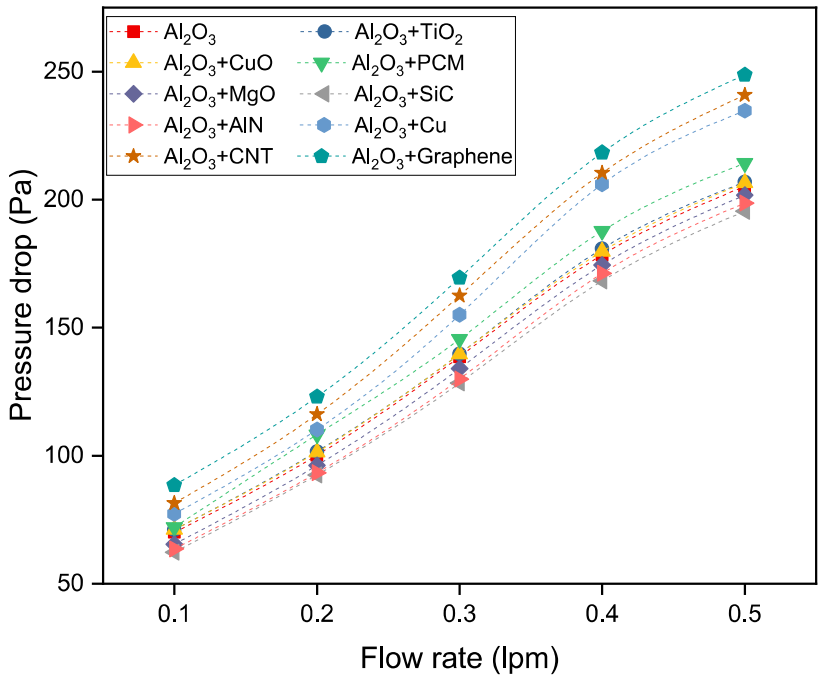

Fig. 4.9 Changing in pressure drop with flow rate for different working fluids

By adding the nanoparticles in the base fluid, improvement in the heat transfer performance is occurred but on the penalty of increment in pressure drop. The penalty in pressure drop by adding nanoparticles with flow rate is shown in Fig. 4.9 for the channel. Generally, the density and viscosity are responsible for the pressure drop increment by adding nanoparticles. The maximum value for pressure drop is found 248.67 N/m^2 for Al_2O_3+graphene/DI water hybrid nanofluid. An increment of about 32.89% is observed for Al_2O_3+graphene dispersed hybrid nanofluid compared to base fluid (DI water). The minimum pressure is found for the Al_2O_3+SiC and Al_2O_3+AlN dispersed hybrid nanofluids. The flow rate (inlet velocity) is also accountable for increment in pressure drop. From the study, it has been justified that the increment in pressure drop can be compromised for all the nanofluids over base fluid.

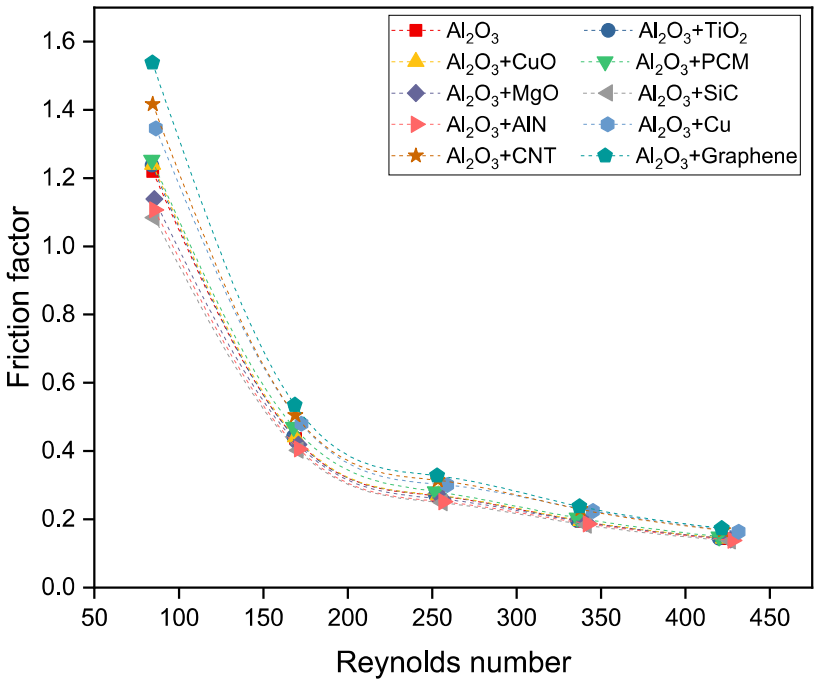

Fig. 4.10 Changing of friction factor with Reynolds number for working fluids

Fig. 4.10 illustrates the changing of friction factor as a function of Re number for different working fluids. The use of all the hybrid nanofluids increases the friction factor in minichannel compared to the base fluid. It is well known that the friction factor decreases with the Reynolds number. At Re=84.5, the maximum value of the friction factor for Al_2O_3+ graphene/DI water nanofluid is approximate 1.53. The deviation of friction factor for different working fluids is significant at lower Reynolds number, as shown in Fig. 4.10. The main reason behind it may be viscosity is predominant at lower Reynolds number. The friction factor for allotropes of carbons dispersed hybrid nanofluid is far away from all others working fluids. It is justified by the fact that the viscosity increases higher with graphene nanoplate and MWCNT due to particle surface area and interparticle attraction. Another reason may be rupturing of the boundary layer is predominant for graphene nanoplate and MWCNT compared to all other nanoparticles.

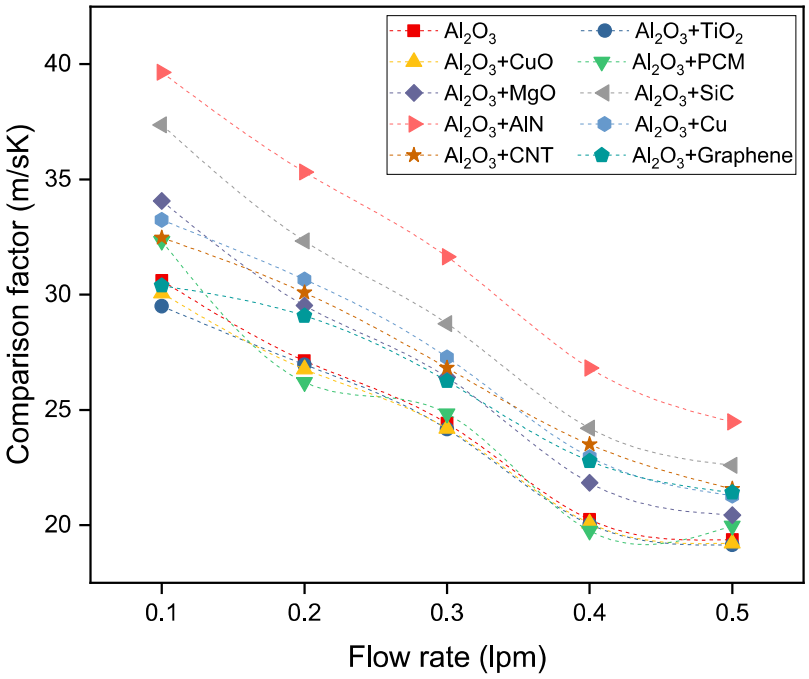

Fig. 4.11 Comparison factor (Heat transfer coefficient to pressure drop ratio, h/Δp) at different flow rates

Fig. 4.11 represents the effect of volumetric flow rates on the comparison factor (ratio of heat transfer coefficient and pressure drop, h/Δp) for different working fluids. h/Δp ratio has a maximum value at a lower flow rate (0.1 lpm) due to the fact that pressure drop increases at a faster rate as compared to heat transfer coefficient. Al_2O_3+AlN based hybrid nanofluid has a maximum h/Δp ratio as compared to all others working fluids in the range of flow rate from 0.1 lpm to 0.5 lpm. h/Δp ratio is for Al_2O_3+graphene based hybrid nanofluid quite less irrespective of high convective heat transfer coefficient. The main reason behind the high pressure drop is the high specific surface area and a higher aspect ratio for graphene. It is also predicted from the figure that h/Δp ratio for Al_2O_3+CuO and Al_2O_3+TiO_2 mixture dispersed hybrid nanofluids has a lower value as approximately the same as Al_2O_3/DI water nanofluid. It is because of the rate of pressure drop increment is higher as compared to enhancement in heat

transfer coefficient at a higher flow rate. PCM dispersed hybrid nanofluid has a minimum h/Δp ratio after 0.2 lpm. At a low flow rate (0.1 lpm), the improvement of the heat transfer coefficient is dominated due to latent heat. So, the heat transfer coefficient to the pressure drop ratio (h/Δp) is high. At 0.2 lpm, no melting of PCM and hence pressured drop dominated. Thus, h/Δp is lower than that of others. At a higher flow rate (0.3-0.5 lpm), negligible enhancement of the heat transfer coefficient occurs, so the value of h/Δp is similar to water.

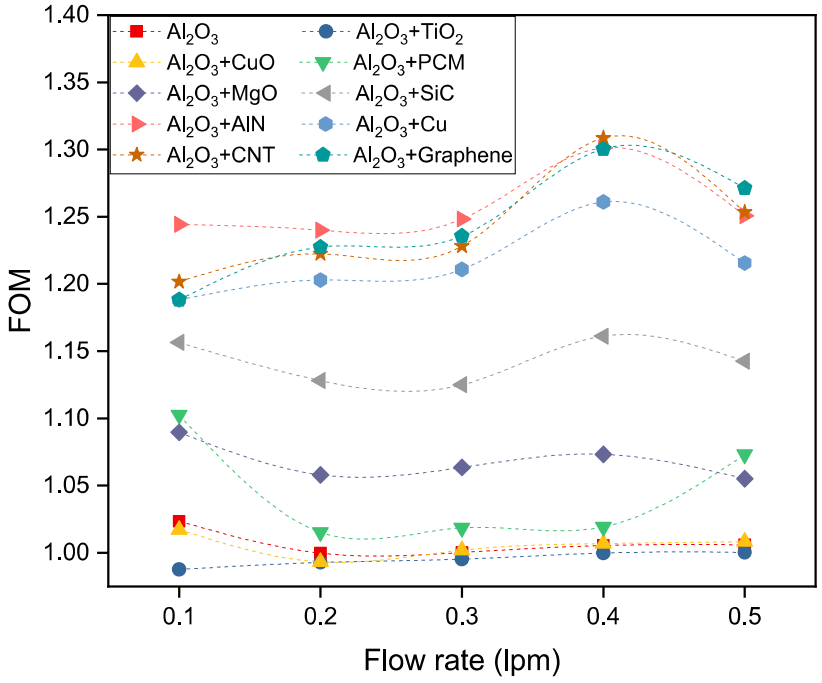

Fig. 4.12 FOM with flow rate for different hybrid nanofluids

To characterize the performance of minichannel heat sink, the figure of merit (FOM) has been used as a comparative criterion of heat transfer improvement versus penalty in pumping power. The acceptance of hybrid nanofluids over conventional fluid for cooling purposes, FOM should meet the criteria above one. The effect of flow rate on the FOM for different coolants is shown in Fig. 4.12. In all the cases, FOM value is above one, so it is interpreted that usage of nanofluid is effective as a coolant compared

to distilled water in minichannel heat sink. It can be concluded that the enhancement in pressure drop is less remarkable as compared to improvement in the heat transfer coefficient. As the thermal conductivity of nanoparticles is increasing, an optimum value of FOM is achieved at 0.4 lpm. Nanoparticles, having low thermal conductivity, did not achieve an optimum point. CuO and TiO_2 dispersed hybrid nanofluids have FOM value of near one.

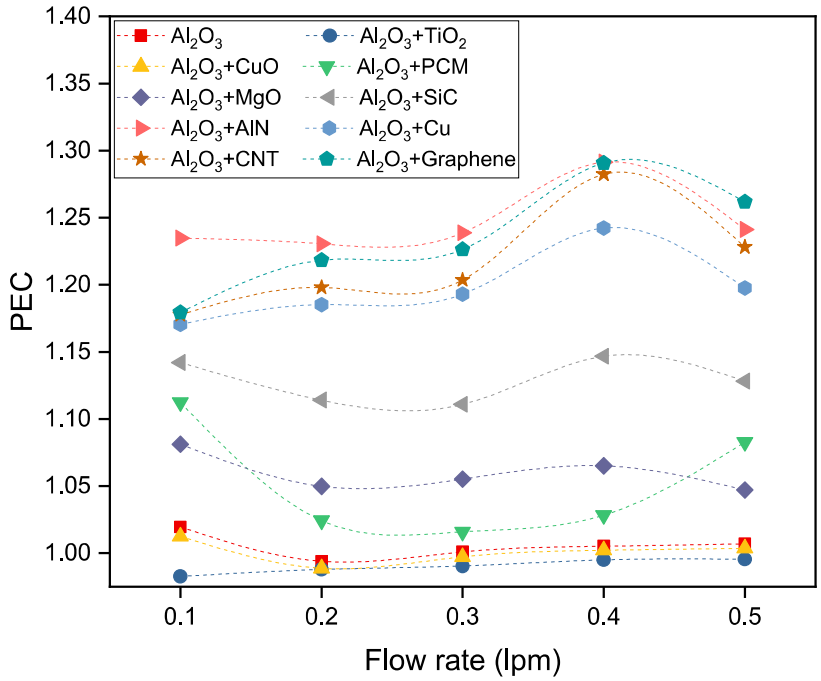

Fig. 4.13 PEC with flow rate number for different working fluids

Fig. 4.13 demonstrates the Performance evaluation criteria (PEC) with the flow rate for different working fluids. It is necessary to evaluate the minichannel heat sink performance based on thermal and flow behavior. So, a term PEC is defined as the thermal efficiency and it is calculated from Eq. 4.21. All the working fluids have PEC more than unity except hybrid nanofluids, which dispersed with nanoparticles having low thermal conductivity.

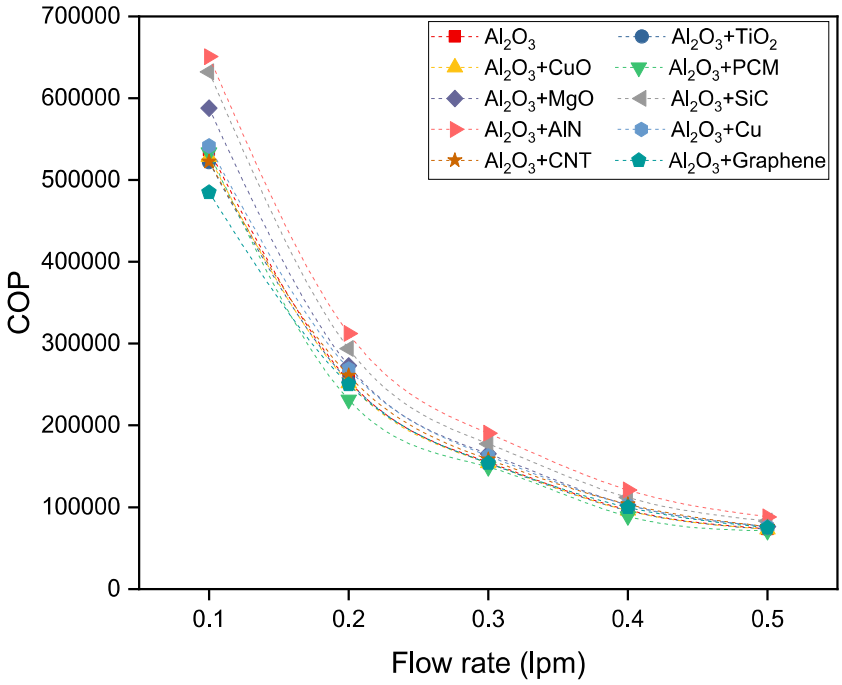

Fig. 4.14 COP with flow rate for different working fluids

The variation of COP with flow rate is illustrated in Fig. 4.14, which shows that COP value goes down with flow rate. The results reveal that the COP increases with the addition of the nanoparticles, except in some cases. This may be due to the increment of viscosity by adding nanoparticles leads to a rise in pumping power. However, Al_2O_3+AlN mixture-based hybrid nanofluid has higher COP as compared to all other coolants.

The total entropy generation rate is the summation of thermal and frictional entropy generation rate. The total entropy generation rate at different flow rates has been shown in Fig. 4.15 for different working fluids. Entropy generation is increasing with the flow rate. Maximum total entropy generation is found for the allotropes of carbon (MWCNT and graphene nanoplates) dispersed hybrid nanofluid at all the flow

rates. Entropy generation depends upon the irreversibility due to heat transfer and pressure drop. Thermal entropy generation for water is higher compared to nanofluids,

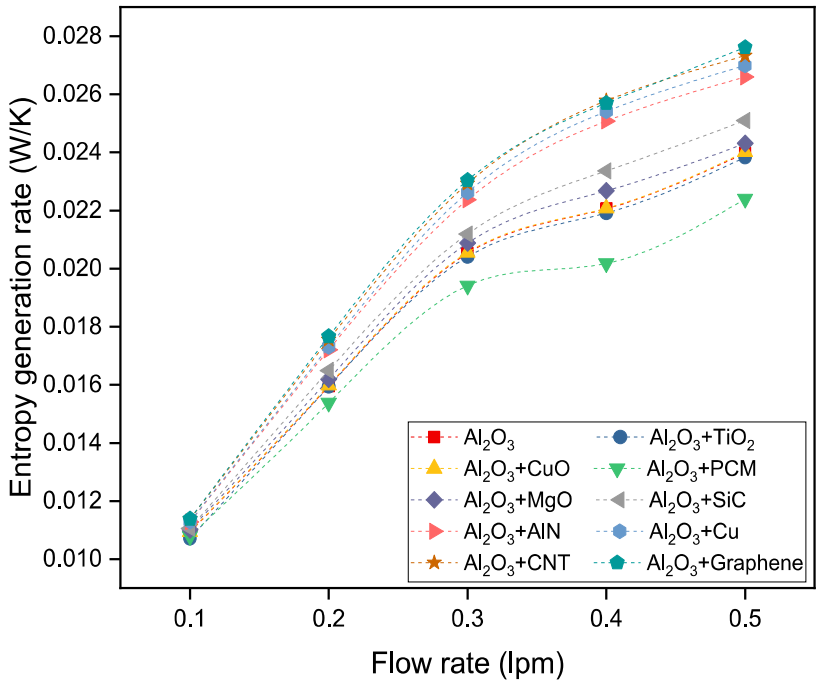

Fig. 4.15 Changing in total entropy generation rate with flow rate for different working fluids

but frictional entropy generation rate increases with the addition of nanoparticles in the base fluid due to friction between the nanoparticles and channel walls. Also, the increase in the flow rate leads to an increment of flow velocity, which further tends to enhance the frictional entropy generation rate. In this experimental work, the overall effect is that the total entropy generation rate increases with flow rate and with nanoparticle addition.

4.4.2 Effect of nanoparticles concentration

The effect of volume concentration on heat transfer coefficient and Nusselt number at a mean condition flow rate (i.e., 0.3 lpm) has been shown in Fig 4.16(a) and

4.16(b), respectively. As the nanoparticle concentration increases from 0.01 vol% to 0.1 vol%, the heat transfer coefficient improved. Maximum enhancement of 11.1% in the heat transfer coefficient is shown for Al_2O_3+CNT based hybrid nanofluid when concentration increased from 0.01 to 0.1 vol% and Al_2O_3+TiO_2 nanofluid has low enhancement in heat transfer coefficient. As the particle concentration increases from

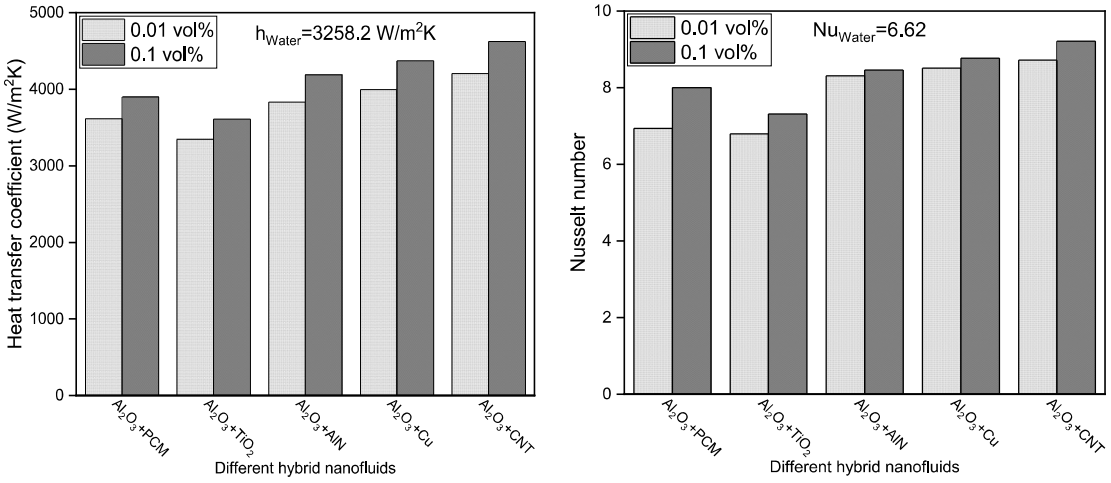

(a) (b)

Fig. 4.16 Effect of volume concentration on (a) heat transfer coefficient and (b) Nusselt number

0.01 to 0.1 vol%, the cost of nanoparticles increases 10 times and the maximum enhancement in the heat transfer coefficient reported only 11.1% (1.1 times). Thus, from an economic point of view, we can conclude that the investigation of higher particle concentration is not significant. Nusselt number follows the same trends as the heat transfer coefficient with nanoparticle concentration.

Fig. 4.17(a-b) shows the effect of volume concentration on pressure drop and friction factor for different hybrid nanofluids at a mean flow rate of 0.3 lpm. It is depicted from the Fig. 4.17(a) that the penalty of pressure drop rises as the particle concentration increases. Al_2O_3+AlN mixture-based hybrid nanofluid has less

enhancement and Al_2O_3+CNT shows maximum penalty in pressure drop. This is due to the cylindrical shape of MWCNT responsible for creating extra viscous flow. The friction factor shows the same response to volume concentration as pressure drop. The friction factor also increases with the rise in volume concentration, as presented in Fig. 4.17(b).

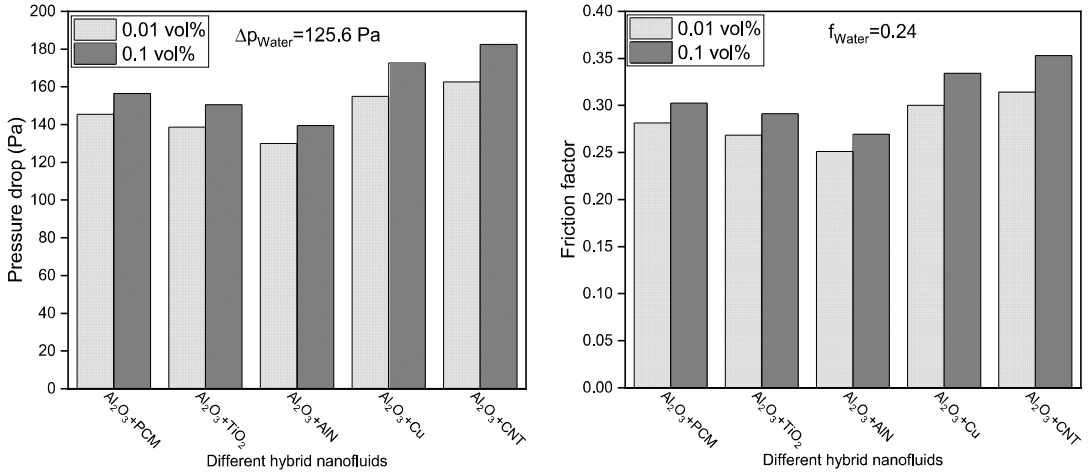

(a) (b)

Fig. 4.17 Effect of volume concentration on (a) pressure drop and (b) friction factor

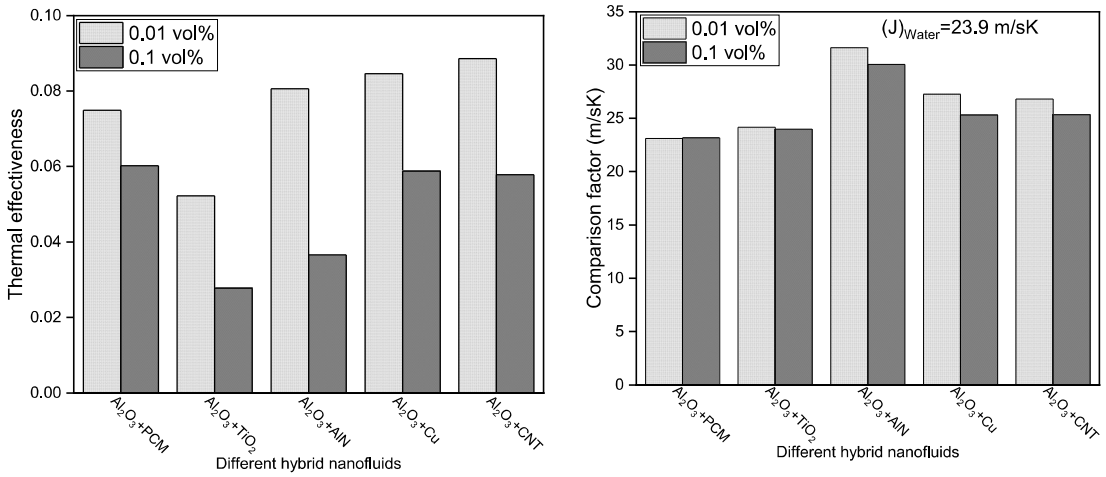

(a) (b)

Fig. 4.18 Effect of volume concentration on (a) thermal effectiveness and (b) comparison factor

The effect of volume concentration on thermal effectiveness and comparison factor (heat transfer coefficient to the pressure drop ratio) at 0.3 lpm is shown in Fig. 4.18a) and 4.18(b), respectively. It can be seen from Fig. 4.18(a), thermal effectiveness value decreases with an increase in the volume concentration from 0.01 vol% to 0.1 vol%. It is because of the temperature difference between outlet and inlet temperature of hybrid nanofluid through the heat sink increases due to increase in volume concentration of nanoparticles in the base fluid. The heat transfer coefficient to pressure drop ratio decreases for all the hybrid nanofluids except PCM dispersed hybrid nanofluid, as shown in Fig. 4.18(b). Thus, we can conclude that pressure drop increases more as compared to the heat transfer coefficient. But in the case of PCM, both the heat transfer coefficient and pressure drop increase at the same rate.

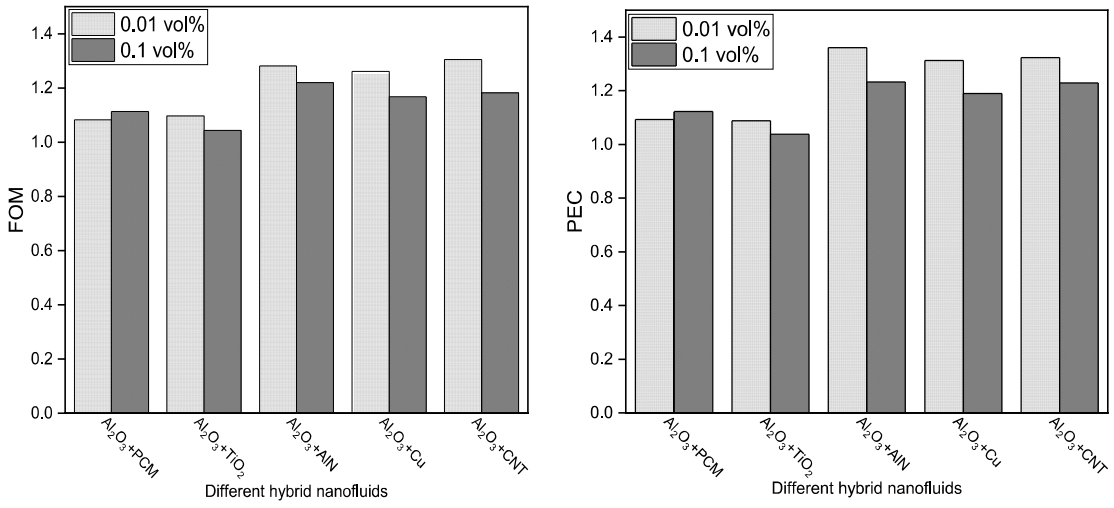

(a) (b)

Fig. 4.19 Effect of volume concentration on (a) figure of merit and (b) performance evaluation criteria

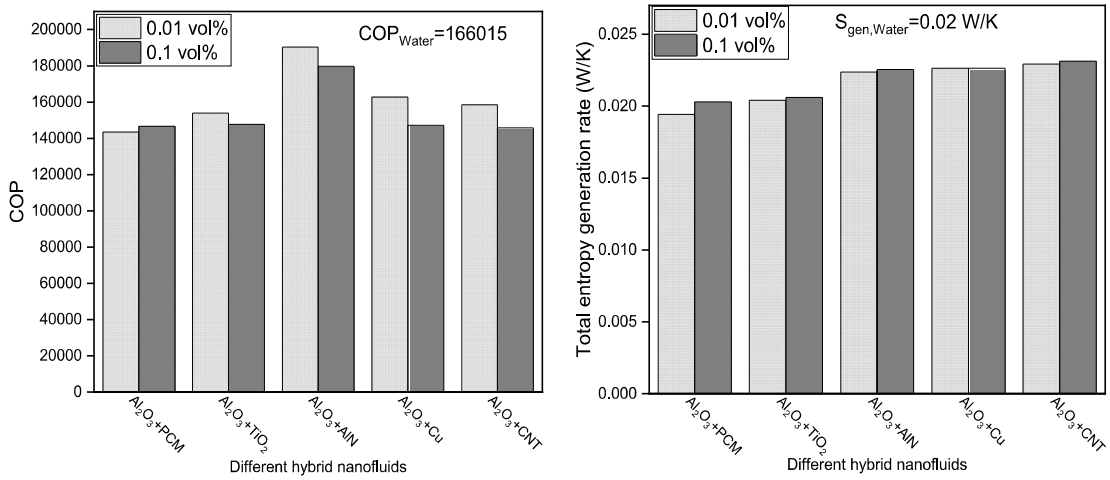

(a) (b)

Fig. 4.20 Effect of volume concentration on (a) coefficient of performance and (b) total entropy generation rate

It can be realized from Fig. 4.19(a-b), FOM and PEC are decreasing as the volume concentration rises from 0.01 vol% to 0.1 vol% for all the hybrid solutions except PCM dispersed hybrid nanofluid. From this, we can reveal that the pressure drop characteristics (pressure drop and friction factor) increase with more rate when compared to heat transfer parameters (heat transfer coefficient and Nusselt number) as volume concentration increasing from 0.01 vol% to 0.1 vol%.

The effect of volume concentration on the coefficient of performance and total entropy generation rate for different combinations of nanoparticles is depicted in Fig. 4.20(a) and 4.20(b), respectively. COP is decreasing for all the hybrid combination nanofluids except PCM dispersed solution, as shown in Fg. 4.20(a). The reason has been deliberated above that pumping power (directly proportional to pressure drop) increases at a more rate compared to heat transfer. But in the case of PCM, as the concentration of PCM increases in solution from 0.01 to 0.1 vol%, then COP increases because it extracted more heat against the penalty of pressure drop. There is no effect of

volume concentration on the total entropy generation rate when it rises from 0.01 to 0.1vol% except PCM dispersed hybrid nanofluid, as depicted in Fig. 4.20(b). The reason to support it that the rise in frictional entropy generation rate is approximately equal to a decrease in thermal entropy generation rate.

4.4.3 Effect of nanoparticle mixing ratio

In this section, the effect of nanoparticle mixing ratio has been discussed on different parameters such as heat transfer coefficient, Nusselt number, pressure drop, FOM, etc. Different mixture ratios of 5:0 to 0:5 are considered. These mixing ratios are in the volume ratios. Al_2O_3 nanoparticle with PCM, TiO_2, MWCNT mixture dispersed nanofluids of 0.01 and 0.1 vol.% concentration has been in the present study. The purpose of showing these results is to find out the optimum mixing ratio.

Fig 4.21 depicts the nanoparticle mixing ratio effect on the heat transfer coefficient for various hybrid nanofluids at different total nanoparticle volume concentrations, volumetric flow rates and heat fluxes. For Al_2O_3+TiO_2 dispersed hybrid nanofluid at a total volume concentration of 0.01 and 0.1 vol%, the heat transfer coefficient is decreasing with the rise in the TiO_2 fraction irrespective of different heat flux and aspect ratio. As the fraction of MWCNT is increasing in the nanofluid, the heat transfer coefficient is continuously increasing and has maximum value for pure MWCNT nanofluid. In the case of Al_2O_3+PCM hybrid nanofluid, Al_2O_3+PCM mixture (equal fraction, i.e., 2.5:2.5) dispersed hybrid nanofluid has maximum value as compared to both pure Al_2O_3 and PCM dispersed nanofluids.

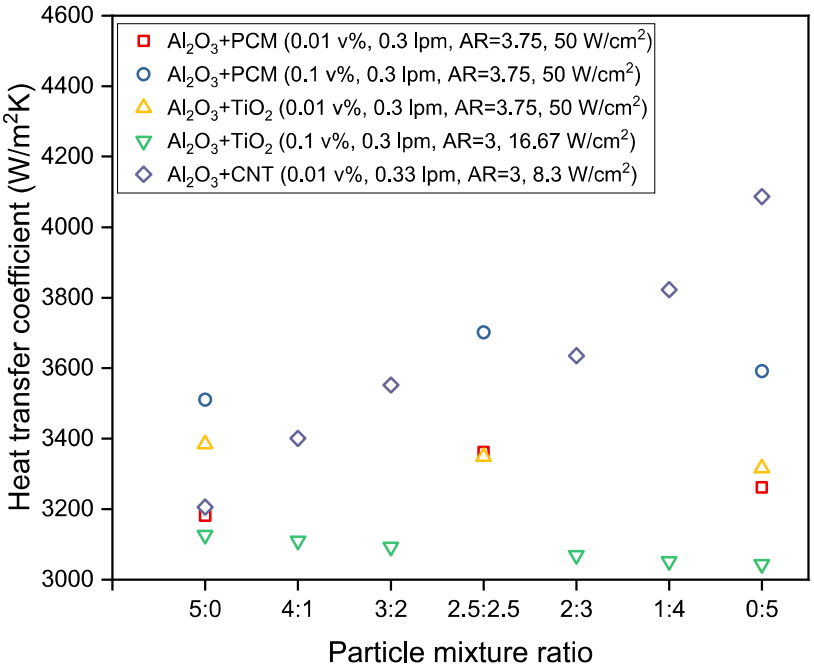

Fig 4.21 Nanoparticle mixing ratio effect on heat transfer coefficient

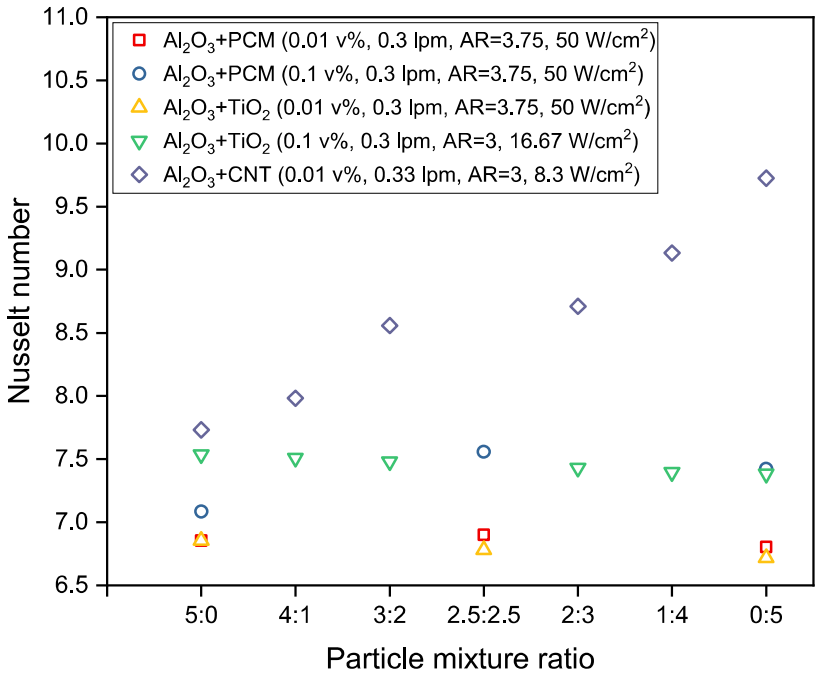

Fig 4.22 Nanoparticle mixing ratio effect on Nusselt number

The effect of mixing ratio on Nusselt number for different hybrid nanofluids is presented in Fig. 4.22. It can be concluded that the Nusselt number shows the same pattern as the heat transfer coefficient. The maximum Nusselt number is found for the

pure MWCNT nanofluid. Al_2O_3+PCM mixture (equal fraction, i.e., 2.5:2.5) hybrid nanofluid at both total volume concentration of 0.01 and 0.1% show maximum Nusselt number when compared to pure Al_2O_3 and PCM nanofluids.

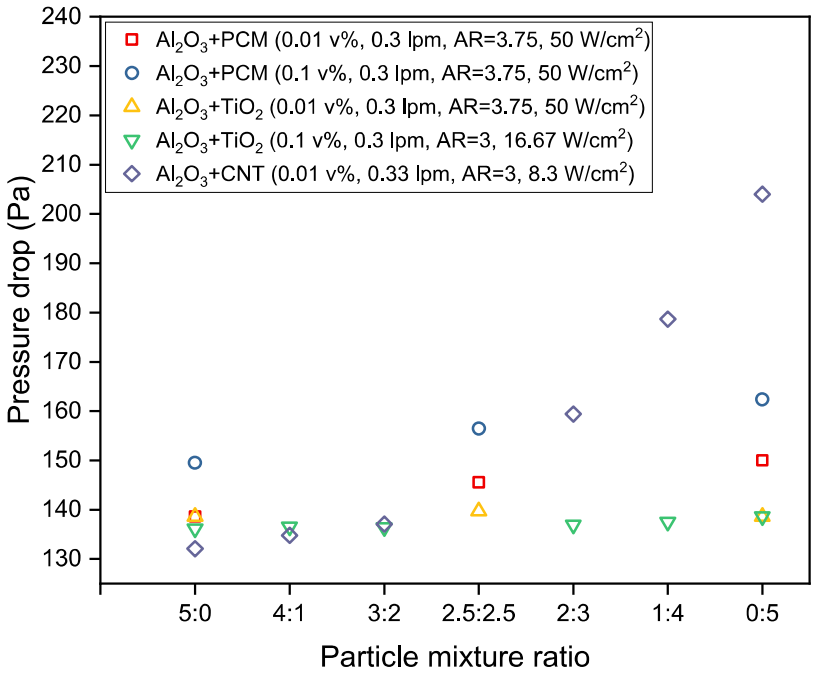

Fig 4.23 Nanoparticle mixing ratio effect on pressure drop

Fig. 4.23 presents the effect of nanoparticle mixing ratio on pressure drop of different hybrid nanofluid in minichannel heat sink. In the case of Al_2O_3-TiO_2 hybrid nanofluid, no significant effect of mixture ratio on pressure drop is found, as there is no significant variation as the TiO_2 fraction rises in the nanofluid irrespective of different aspect ratio, heat flux and total nanoparticles volume concentration. As the fraction of PCM in hybrid nanofluid is increasing, the pressure drop is increasing and has a maximum pressure drop for PCM nanofluid. For MWCNT suspended hybrid nanofluid, pressure drop increasing drastically when MWCNT fraction is more than 50% in the hybrid nanofluid. The effect of the particle mixing ratio of various hybrid nanofluids on

friction factor has been depicted in Fig 4.24 at different total volume concentrations, aspect ratio and heat flux. The friction factor shows the same pattern as pressure drop with nanoparticle mixing ratio. There is not observed any optimum mixing ratio for pressure drop and friction factor.

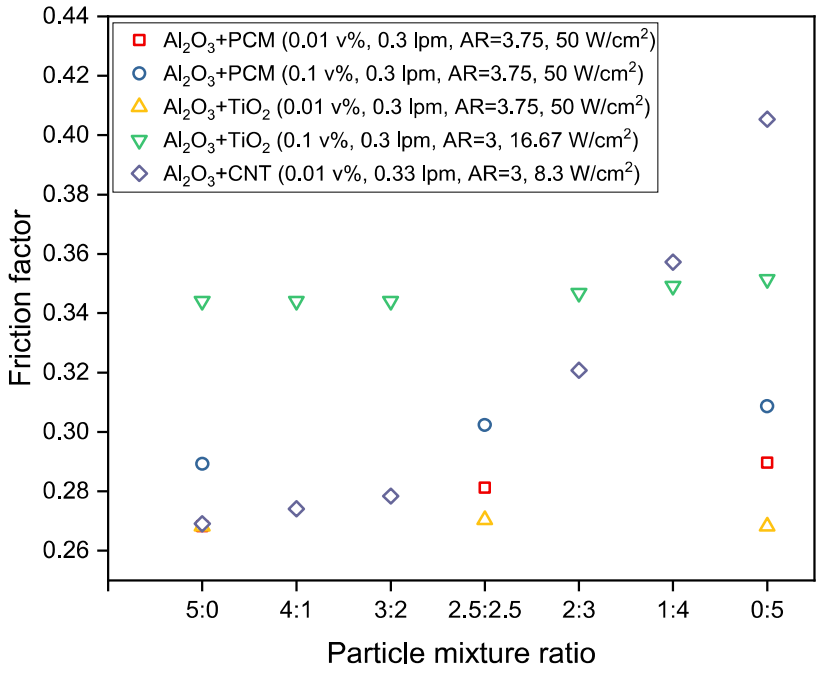

Fig 4.24 Nanoparticle mixing ratio effect on friction factor

Fig. 4.25 presents the nanoparticle mixing ratio effect on the thermal effectiveness of minichannel heat sink using different hybrid nanofluids. It can be seen that thermal effectiveness for Al_2O_3+TiO_2 at 0.01 vol% is not showing any optimum effectiveness. But when total volume concentration rises from 0.01 to 0.1 vol%, it is decreasing and starts increasing after mixing ratio of 1.4. In the case of Al_2O_3+PCM, hybrid nanofluids show an optimum point for an equal fraction (i.e., 2.5:2.5) at 0.01 vol%. CNT dispersed hybrid nanofluid has increasing, decreasing and then increasing trend.

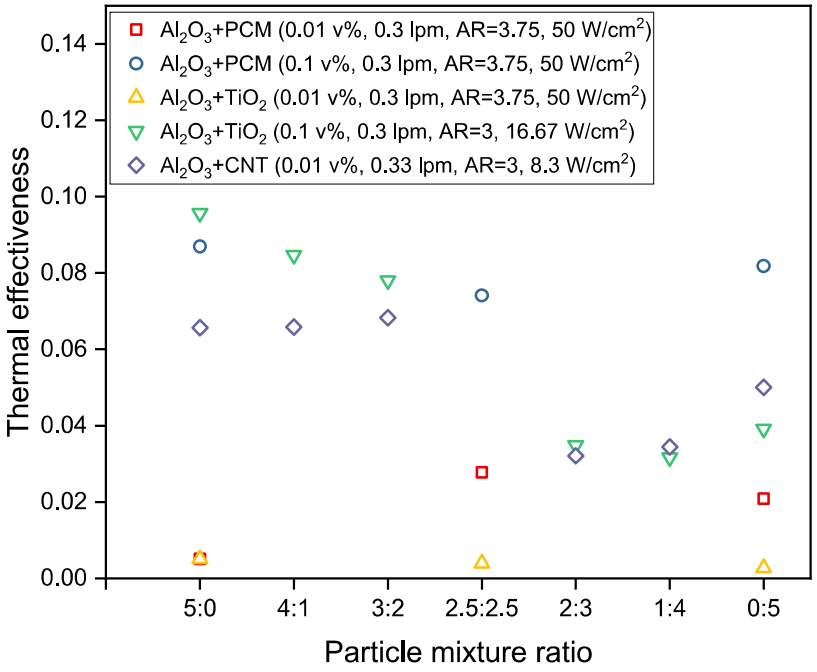

Fig 4.25 Nanoparticle mixing ratio effect on thermal effectiveness

The effect of nanoparticle mixing ratio on comparison factor (heat transfer coefficient to pressure drop ratio) has been shown in Fig. 4.26 for various combinations of nanoparticles-based hybrid nanofluid in minichannel heat sink. From here, it can be seen that there is no optimum point for all the combinations except Al_2O_3+CNT hybrid nanofluid. We have revealed that there is a negligible effect of mixture ratio for similar particles (spherical-spherical) and oxide-PCM combination dispersed hybrid nanofluid. From the figure, it is concluded that 3:2 ratio is the optimum mixture ratio for the Al_2O_3-MWCNT (spherical-cylindrical) nanoparticle combination in minichannel heat sink. It is due to pressure drop rises as the fraction of MWCNT increases in the hybrid nanofluid. The reason for the increase in pressure drop is because of its high specific surface area due to the higher aspect ratio for MWCNT, as discussed above. Thus, it can be concluded that the combination of different types of nanoparticles (i.e., spherical-cylindrical) shows optimum particle ratio for best hydrothermal performance.

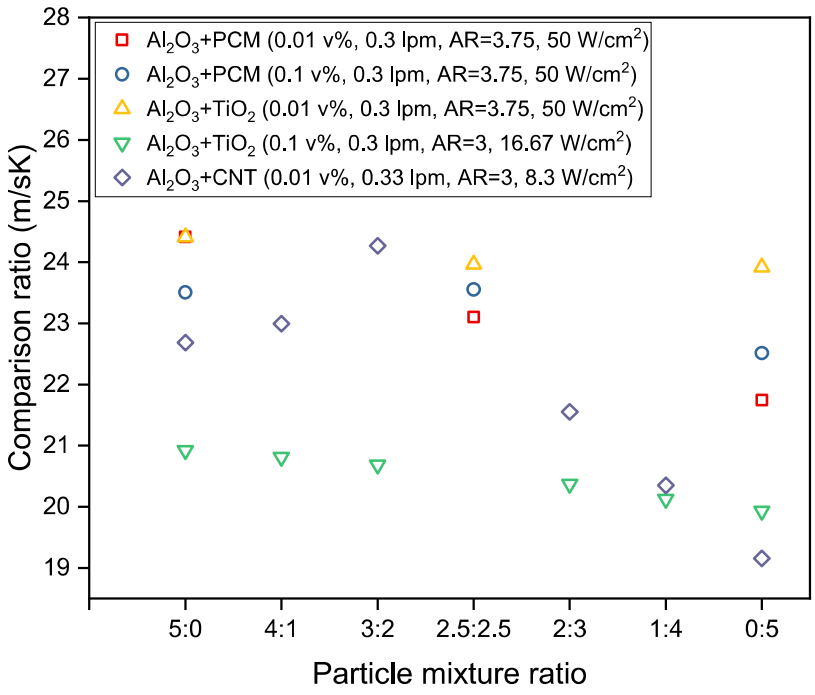

Fig 4.26 Nanoparticle mixing ratio effect on comparison factor

Fig. 4.27 presents the particle mixing ratio effect on the figure of merit for different hybrid nanofluids in minichannel heat sink. It can be concluded that the pattern followed by different hybrid nanofluids would not be the same because of the different combination of nanoparticles is considered. FOM for Al_2O_3+TiO_2 dispersed hybrid nanofluid does not show any optimum point. It has decreasing trends as the TiO_2 fraction in hybrid nanofluid is increasing. Al_2O_3+PCM hybrid nanofluid at 0.01 vol% has decreasing trends when the PCM fraction goes rises in particle mixing ratio, but it has an optimum value at ratio 2.5:2.5 when total volume concentration is 0.1%. CNT dispersed hybrid nanofluid has increasing-decreasing-increasing trends with a rise in CNT fraction in a hybrid nanofluid. Performance evaluation criteria of various hybrid nanofluids shows the same trend with particle mixing ratio as the figure of merit presented in Fig. 4.28. The Al_2O_3+TiO_2 shows decreasing trends because the friction factor ratio (i.e., the ratio of nanofluid friction factor to base fluid friction factor) does

not change and the Nusselt number ratio (i.e., the ratio of nanofluid Nusselt number to base fluid Nusselt number) is decreasing with the rise in TiO_2 fraction in the hybrid nanofluid.

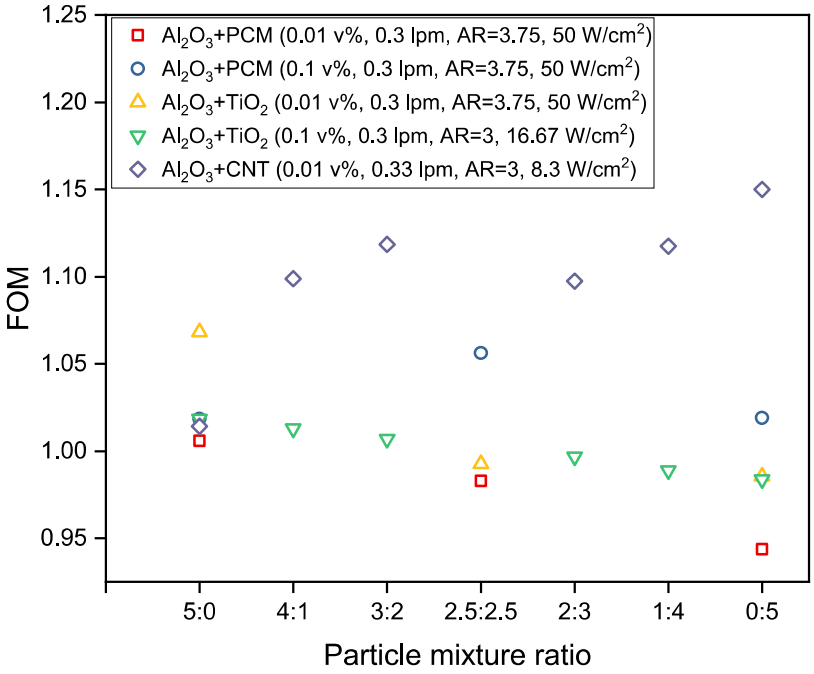

Fig 4.27 Nanoparticle mixing ratio effect on figure of merit

Fig. 4.29 depicts the effect of nanoparticle mixing ratio on the coefficient of performance of various hybrid nanofluids in minichannel heat sink. It can be seen that the COP of Al_2O_3+TiO_2 hybrid nanofluid at 0.01 and 0.1vol% is decreasing as the TiO_2 fraction rises. In the case of Al_2O_3+PCM dispersed hybrid nanofluid, COP goes down when PCM fraction rises. This is support by the fact that as PCM fraction rises, the increment in pumping power dominates over heat transfer. Al_2O_3+CNT shows an optimum point at 3:2 ratio. COP increases up to ratio 3:2 after this free fall occurs. It is because of the rise in CNT fraction in the hybrid nanofluid. As the fraction of CNT rises, the rate of increment in pumping power is more as compared to heat transfer.

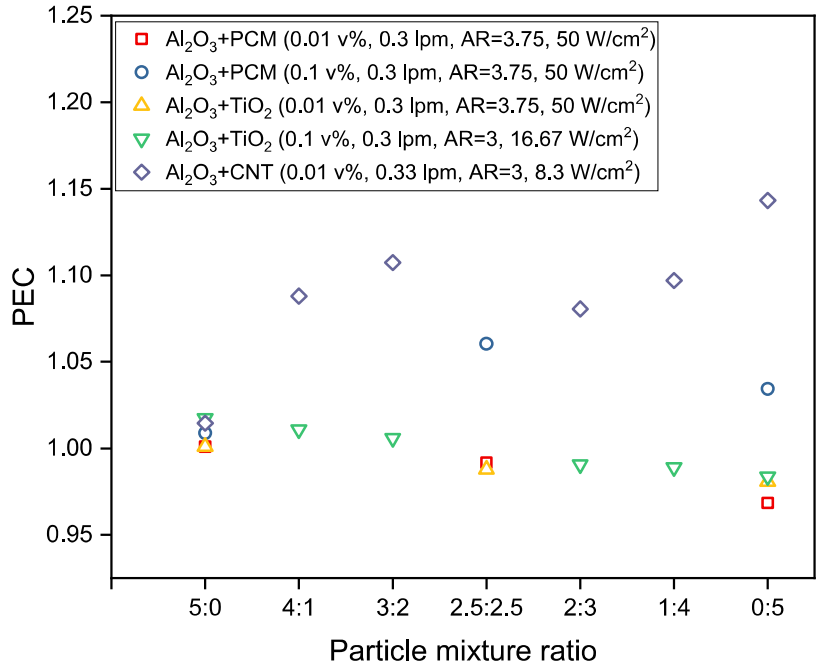

Fig 4.28 Nanoparticle mixing ratio effect on performance evaluation criteria

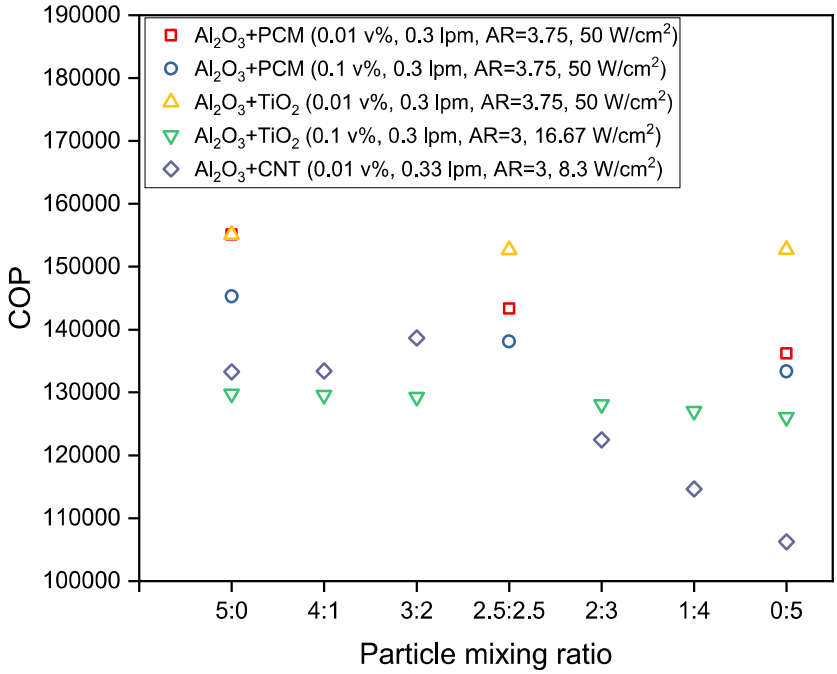

Fig 4.29 Nanoparticle mixing ratio effect on coefficient of performance

Total entropy generation rate variation with particle mixing ratio in hybrid nanofluid is depicted in Fig. 4.30. There is no significant effect on the total entropy generation rate for TiO_2 dispersed hybrid nanofluid at a total volume concentration of

0.01%. But as the volume concentration rises to 0.1vol%, the total entropy generation rate is higher for pure TiO_2 nanofluid as compared to pure Al_2O_3 nanofluid. For Al_2O_3+PCM dispersed hybrid nanofluid, the total entropy generation rate falls with a rise in PCM fraction. The total entropy generation rate is continuously increasing for Al_2O_3+CNT dispersed hybrid nanofluid as CNT fraction upsurges because of the dominance of increment in thermal entropy generation rate and frictional entropy generation rate.

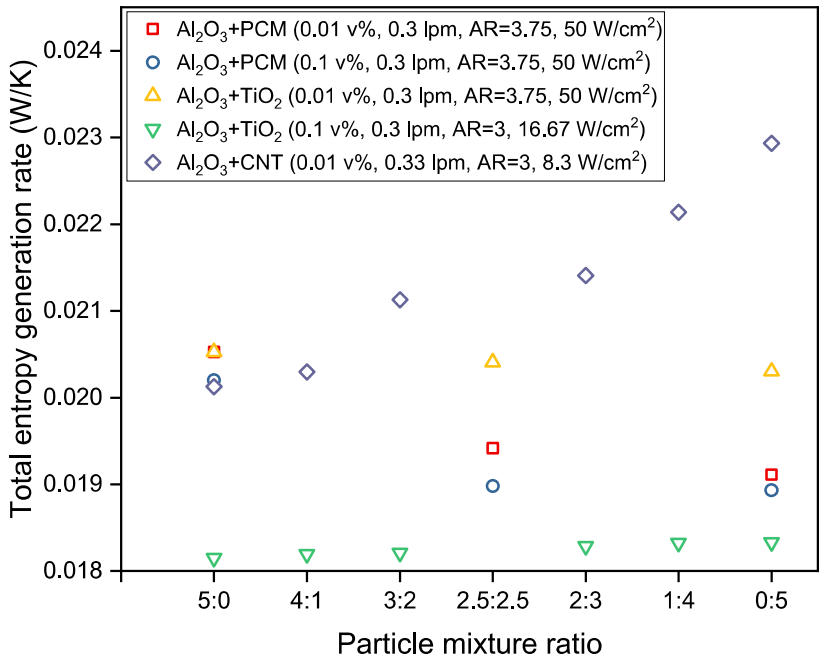

Fig 4.30 Nanoparticle mixing ratio effect on total entropy generation rate

4.4.4 Effect of fluid inlet temperature

In the present investigation, the inlet temperature is varied (20 °C to 40 °C) for the consideration of a wide range of atmosphere temperature variation along with the sustainability and flexibility of the current study globally. Constant temperature bath having synchronized heating and cooling provisions before flowing into the channel is employed for maintaining these temperatures. With the increase in inlet temperature, thermal conductivity and specific heat of nanofluid increases. This enhancement in

thermal conductivity and specific heat has been taken into account when calculating the heat transfer coefficient and Nusselt number. Fig. 4.31 represents the effect of inlet temperature on the heat transfer coefficient and Nusselt number at the mean flow rate (i.e., 0.3 lpm). Fig. 4.31(a) shows that fluid inlet temperature has a positive effect on the heat transfer coefficient. The heat transfer coefficient is increased in the range of 4.2-10.34% when the temperature of working fluids is increased from 20°C to 40°C. The heat transfer enhancement is considerably improved at higher working temperature because of the improvement of thermal properties. The increment of the thermal conductivity of nanofluids is more meaningful at higher operating temperature. Enhancement in thermal conductivity, which is dependent on temperature, may be another possible advantage for using the nanofluids as the high-temperature coolants. A maximum improvement of 10.34% is found for the Al_2O_3+SiC/water hybrid nanofluid. Nusselt number follows the same pattern as the heat transfer coefficient with respect to fluid inlet temperature, as shown in Fig. 4.31(b).

The effect of inlet temperature on pressure drop and friction factor depicts in Fig. 4.32(a) and Fig 4.32(b), respectively. Pressure drop and friction factor both decrease with inlet temperature due to a decrease in viscosity. As the temperature increases from 20^{o}C to 40^{o}C, a decrement of 10.15% has been observed in pressure drop for Al_2O_3+MWCNT dispersed hybrid nanofluid. The friction factor shows the same trends as pressure drop with fluid inlet temperature.

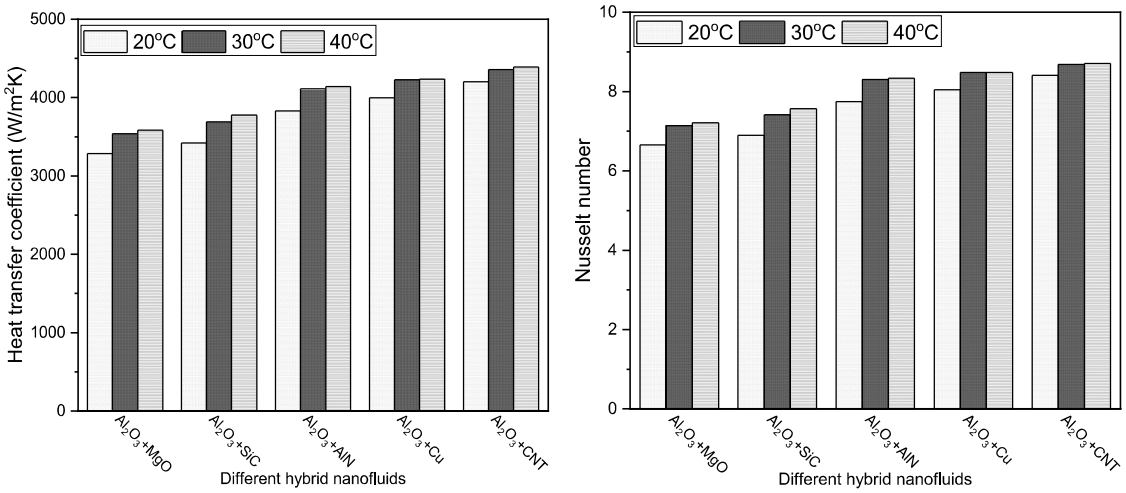

(a) (b)

Fig. 4.31 Variation of (a) heat transfer coefficient and (b) Nusselt number with fluid inlet temperature

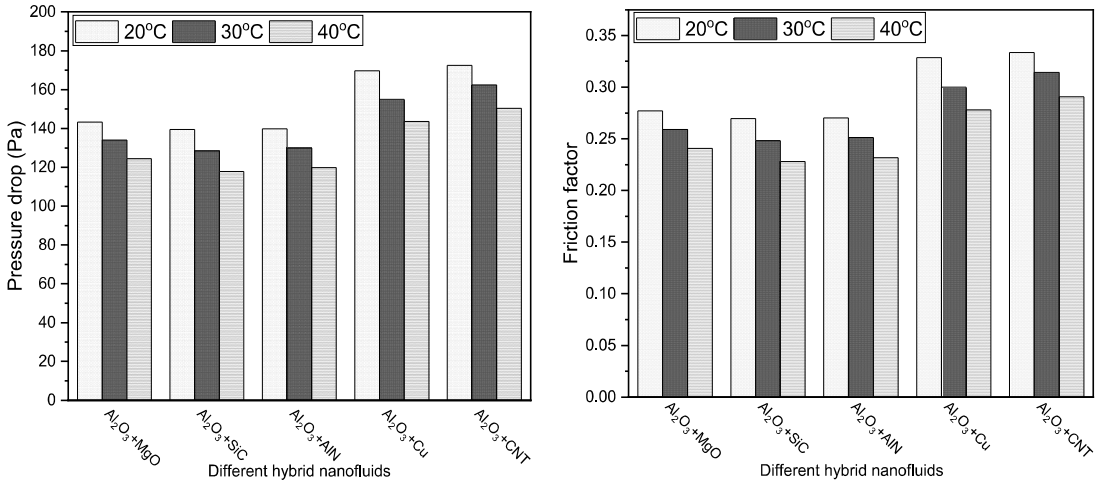

(a) (b)

Fig. 4.32 Variation of (a) pressure drop and (b) friction factor with fluid inlet temperature

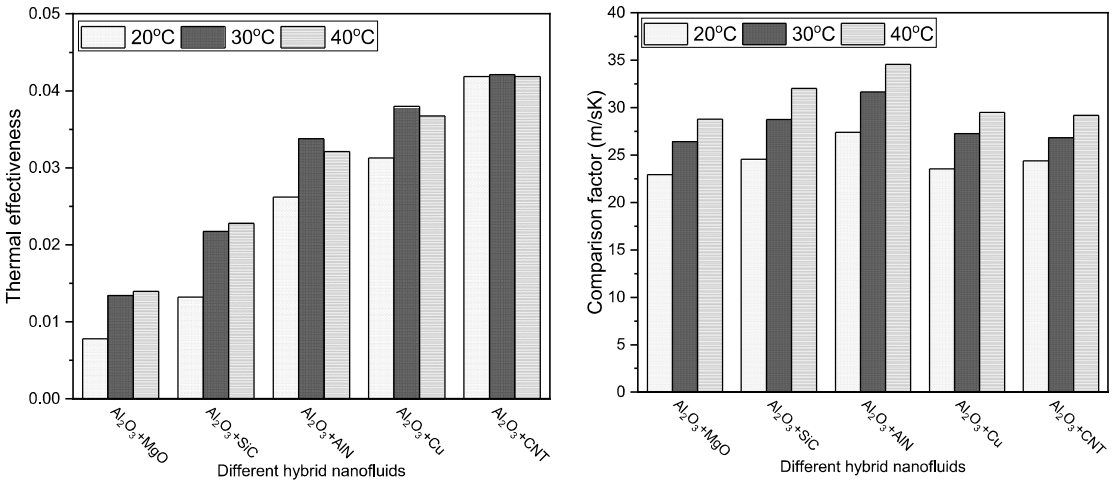

(a) (b)

Fig. 4.33 Variation of (a) thermal effectiveness and (b) comparison factor with fluid inlet temperature

Thermal effectiveness and comparison factor (heat transfer coefficient to the pressure drop ratio) are represented in Fig. 4.33. For MgO and SiC dispersed hybrid nanofluids, thermal effectiveness rises with inlet temperature. For AlN and Cu dispersed hybrid nanofluids, thermal effectiveness first increases from 20°C to 30°C and decreases from 30°C to 40°C, as shown in Fig. 4.33(a). But there is no effect of inlet temperature on CNT dispersed hybrid nanofluids. Comparison factor increases with the rise in temperature, as shown in Fig. 4.33(b). This because of an increase in heat transfer and a decrease in pressure drop with inlet temperature. For MgO and AlN dispersed hybrid nanofluids, FOM is not changing with temperature. It is because the increment in heat transfer coefficient and decrement in pressure drop are in the same ratio for MgO and AlN dispersed hybrid nanofluids.

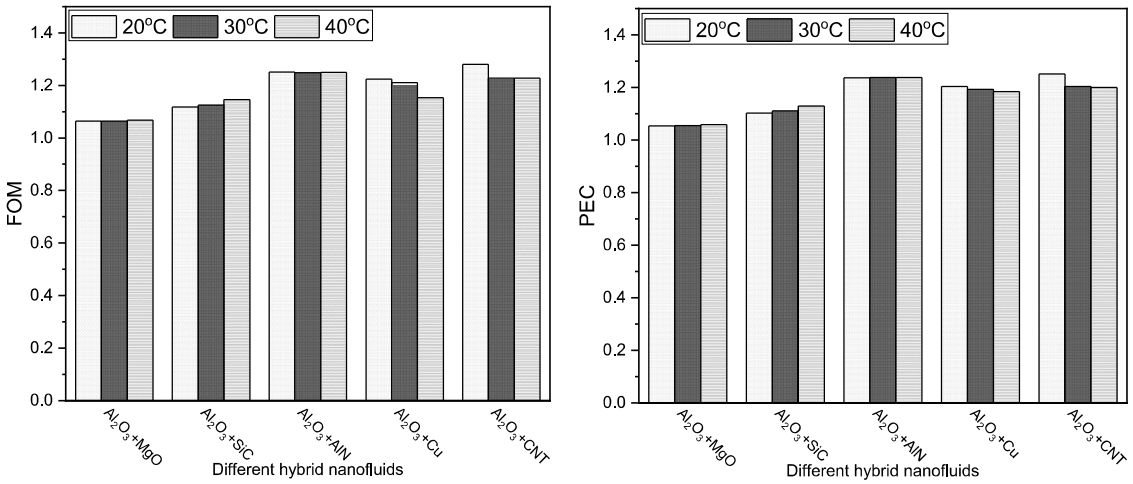

(a) (b)

Fig. 4.34 Variation of (a) figure of merit and (b) performance evaluation criteria with fluid inlet temperature

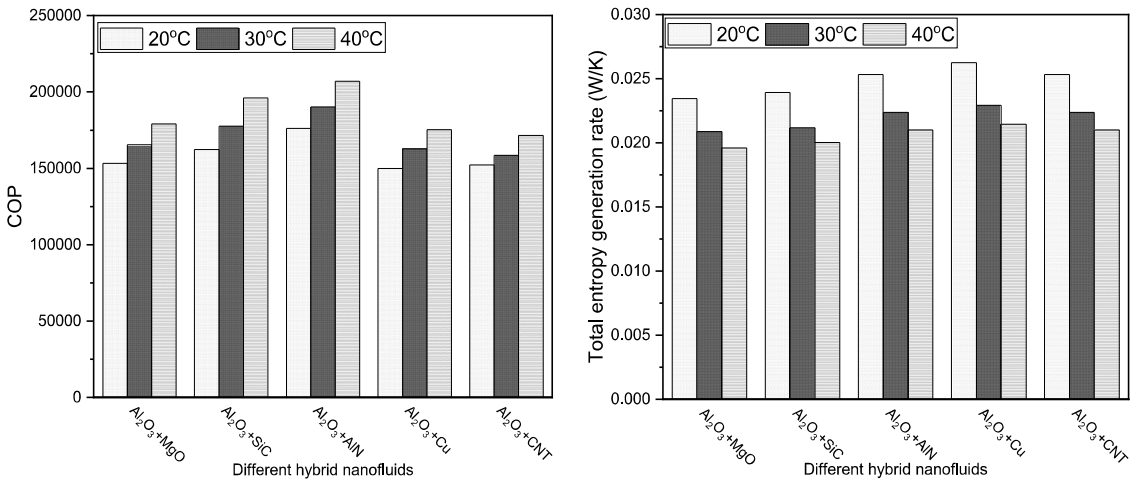

(a) (b)

Fig. 4.35 Variation of (a) coefficent of performance and (b) total entropy generation rate with fluid inlet temperature

The variation of FOM and PEC for different hybrid nanofluids at various inlet temperatures is shown in Fig. 4.34(a) and 4.34(b), respectively. It can be seen that for most of the working fluids, there is no significant variation in FOM and PEC. FOM for

Cu dispersed hybrid nanofluid is decreasing with inlet temperature. Al_2O_3+CNT/water hybrid nanofluid show a decrement in PEC from 20°C to 30°C but no effect from 30°C to 40°C.

Variation of COP and total entropy generation rate with fluid inlet temperature are shown in Fig. 4.35. COP is increasing with the rise in temperature because of an increase in heat transfer and a decrease in pumping power (related to pressure drop) with inlet temperature, as shown in Fig. 4.35(a). The total entropy generation rate is decreasing with fluid inlet temperature for all the hybrid nanofluids as depicts in Fig. 4.35(b). The reason may be that friction entropy generation rate decreases at a faster rate as compared to increment in thermal entropy generation rate.

4.4.5 Effect of heat flux

In this section, the effect of heat flux on different parameters is examined. Changing of heat transfer coefficient and Nusselt number at various heat flux for different hybrid nanofluids are shown in Fig. 4.36. Heat transfer coefficient increases for all the hybrid nanofluids with a rise in heat flux to minichannel heat sink, as shown in Fig. 4.36(a). An enhancement of range from 6.9% to 10.8% has been found for all studied hybrid nanofluids when heat flux rises from 33.33 W/cm^2 to 66.67 W/cm^2. With the rise in heat flux for the same heat transfer area, the heat transfer would increase, which may be responsible for increasing the temperature difference between the bottom wall of the heat sink and channel. An enhancement of 10.8% occurred for PCM dispersed hybrid nanofluid. The same positive effect of heat flux has been revealed for Nusselt number as presents in Fig. 4.36(b).

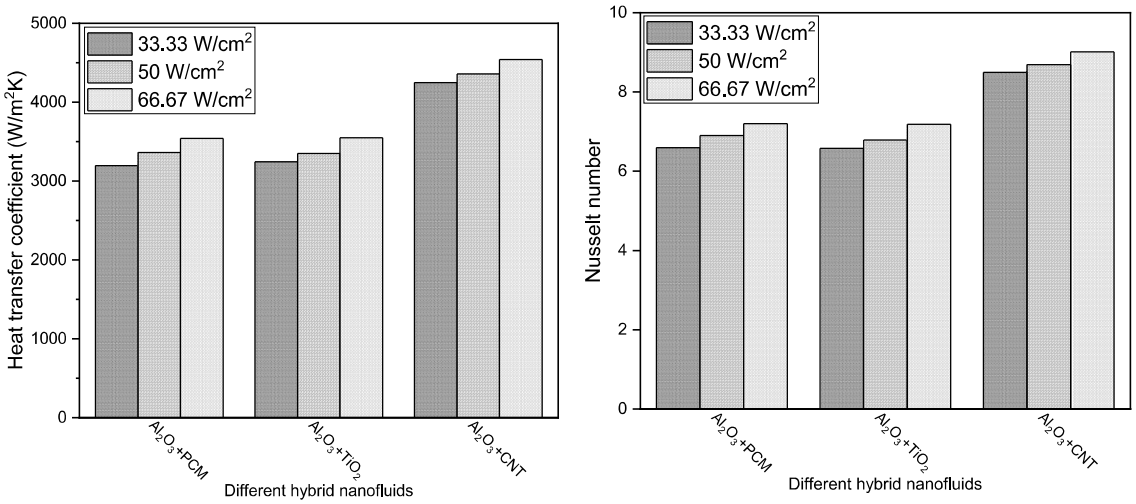

(a) (b)

Fig. 4.36 Changing of (a) heat transfer coefficient and (b) Nusselt number with heat flux

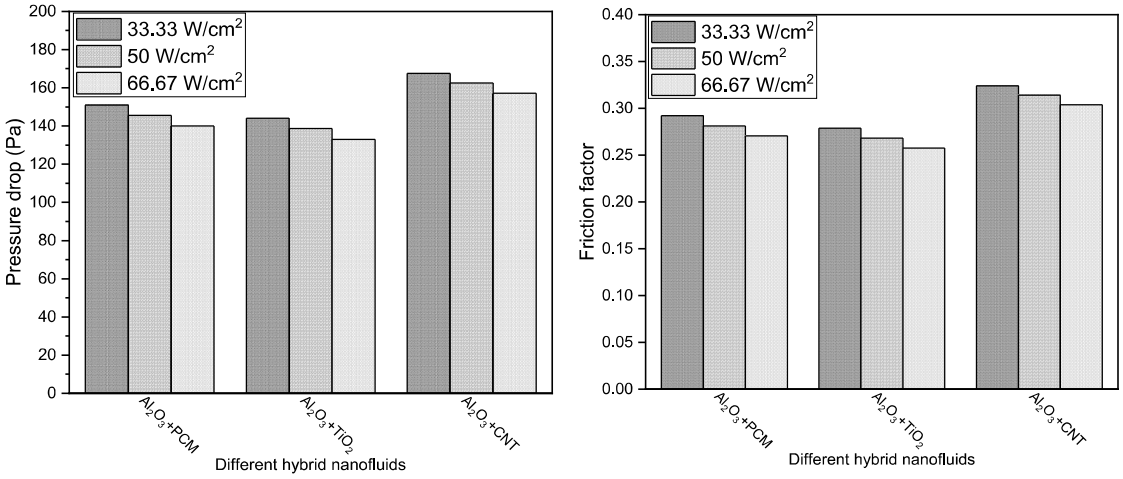

(a) (b)

Fig. 4.37 Changing of (a) pressure drop and (b) friction factor with heat flux

Changing of pressure drop and friction factor with increases in heat flux at 0.3 lpm are presented in Fig. 4.37(a) and 4.37(b), respectively. It can be seen that the pressure drop and friction factor is decreasing with the rise in heat flux. A decrement of 6.7% is observed for TiO_2 dispersed hybrid nanofluid when heat flux increases from 33.33

W/cm^2 to 66.67 W/cm^2 due to a decrease in viscosity. The friction factor is decreasing by 7.6 % for PCM dispersed hybrid nanofluid with a rise in heat flux.

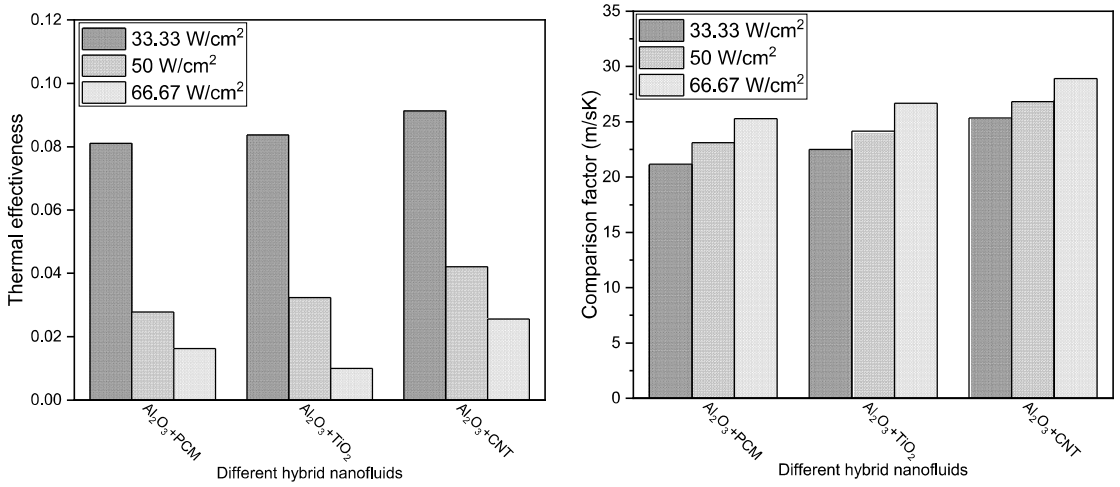

(a) (b)

Fig. 4.38 Changing of (a) thermal effectiveness and (b) comparison factor with heat flux

Thermal effectiveness for all the hybrid nanofluids decreases with an increase in heat flux, as shown in Fig. 4.38(a). This is due to an increase in temperature difference between the inlet and outlet of the hybrid nanofluid when passing through the minichannel as compared to base fluid (DI water) when heat flux rises. A decrement of 79.9% in thermal effectiveness is observed for Al_2O_3+PCM hybrid nanofluid when heat flux rises from 33.33 W/cm^2 to 66.67 W/cm^2. Fig. 4.38(b) presents the effect of heat flux on comparison factor (heat transfer coefficient to the pressure drop ratio) for different hybrid nanofluids. It can be seen that the heat transfer coefficient to the pressure drop ratio increases with the rise in heat flux. The reason is supported that the heat transfer coefficient is increasing and pressure drop is decreasing with the rise in heat flux.

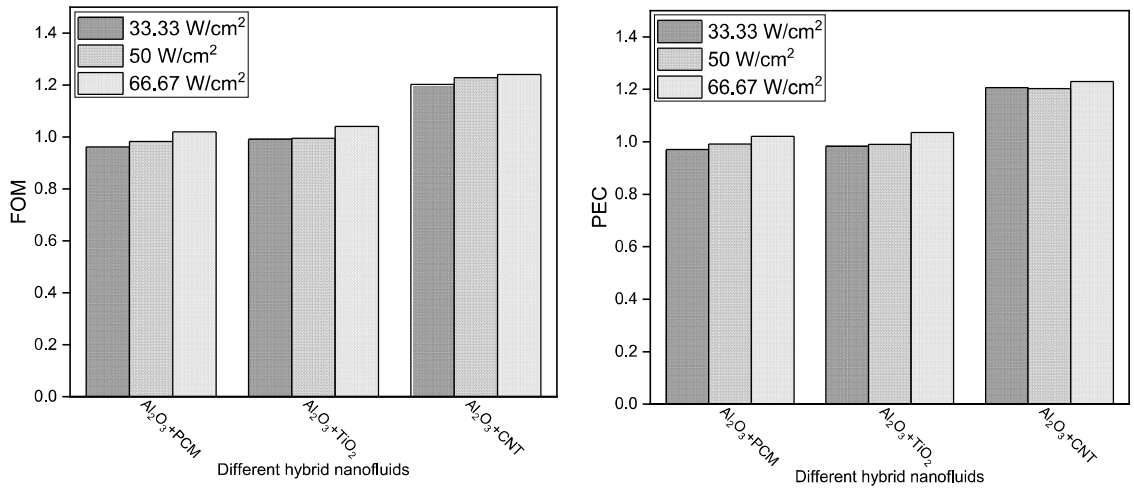

(a) (b)

Fig. 4.39 Changing of (a) figure of merit and (b) performance evaluation criteria heat with flux

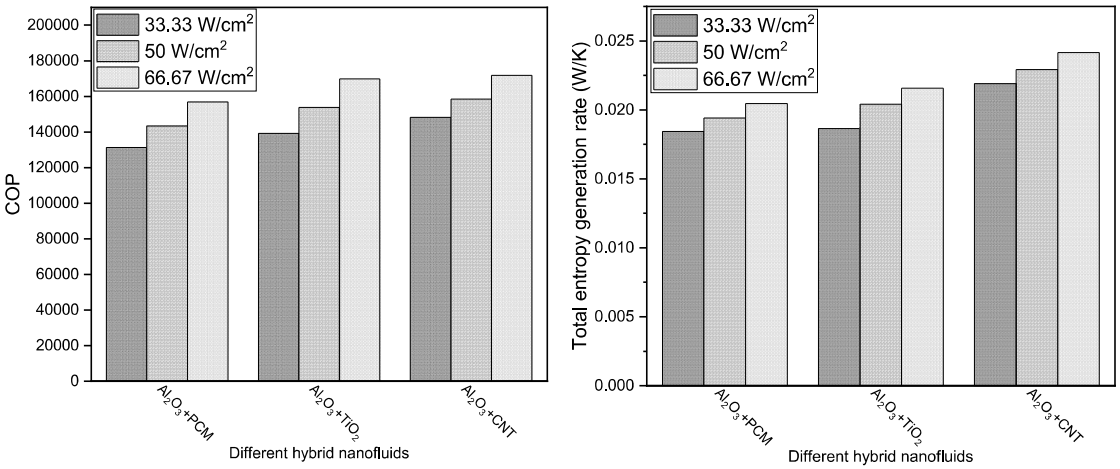

(a) (b)

Fig. 4.40 Changing of (a) coefficent of performance and (b) total entropy generation rate with heat flux

The effect of heat flux on FOM and PEC for different hybrid mixture suspension is shown in Fig 4.39(a) and 4.39(b), respectively. A maximum of 6.2% enhancement in FOM is observed for CNT dispersed hybrid nanofluid when heat flux rises from 33.33

W/cm^2 to 66.67 W/cm^2. Also, at low heat flux, TiO_2 and PCM dispersed hybrid nanofluids, FOM and PEC have to value less than one. Thus, it recommended using hybrid nanofluids at high heat flux.

Fig. 4.40(a) presents the effect of heat flux on COP for different mixture based hybrid nanofluid. The heat transfer rate will increase when the heat flux on the same heat transfer area rises. This leads to an increase in the temperature difference between the bottom of the heat sink and the bottom of the channel. Also, for the same flow rate, the temperature difference between the inlet and outlet of working fluid through minichannel is increased with an increase in heat transfer rate. As the heat flux increases from 33.33 W/cm^2 to 66.7 W/cm^2, thermal entropy generation dominates over friction entropy generation. So, from Fig. 4.40(b), it can be illustrated that the total entropy generation rate increases with increases in heat flux from 33.33 W/cm^2 to 66.7 W/cm^2.

4.4.6 Effect of channel aspect ratio

The effect of aspect ratio on heat transfer coefficient and Nusselt number at 0.3 lpm is depicted in Fig. 4.41(a) and 4.41(b), respectively. As it is well known that if the channel cross-section is decreased, then fluid velocity increased. Increased fluid velocity increases fluid momentum flow in the axial direction, resulting in a thinning of the boundary layer, which increases convective heat transfer. From Fig. 4.41(a), it is shown that the heat transfer coefficient is maximum for the low aspect ratio (i.e., AR=2.5). As the channel wall absorbs heat continuously from the bottom of the heat sink, the fluid momentum is also followed by a bulk transfer of heat from the wall to the maximum extent of the fluid stream, thus increasing the mean temperature of the fluid stream. As a consequence, the change in fluid velocity induces a change in convective heat transfer tends to increase in Nusselt number as presents in Fig. 4.41(b). Maximum

enhancement of 19.66% is observed for TiO_2 dispersed hybrid nanofluid when the aspect ratio decreases from 5 to 2.5.

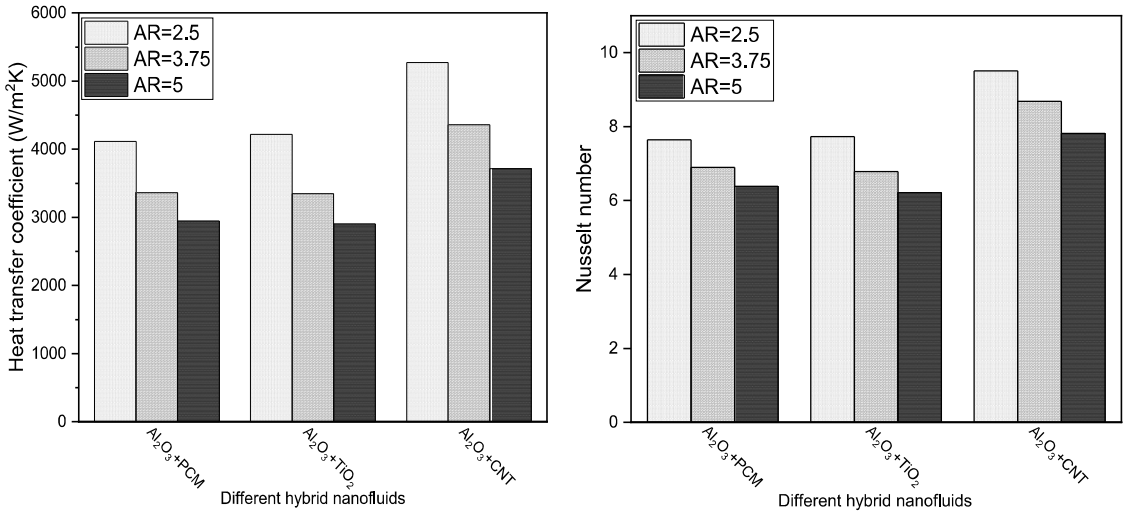

(a) (b)

Fig. 4.41 Effect of channel aspect ratio on (a) heat transfer coefficient and (b) Nusselt number

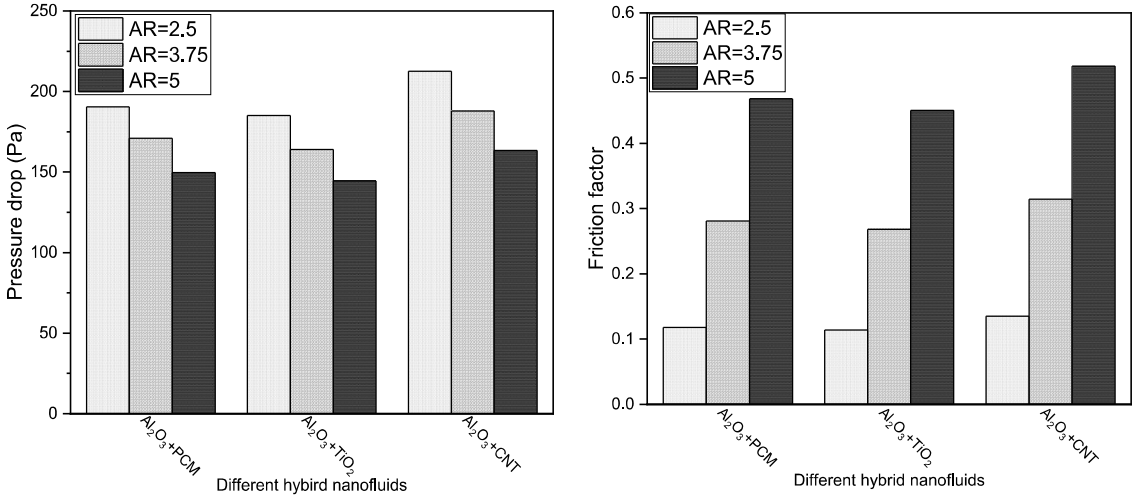

(a) (b)

Fig. 4.42 Effect of channel aspect ratio on (a) pressure drop and (b) friction factor

Fig. 4.42 (a-b) presents the effect of channel aspect ratio on pressure drop and friction factor at 0.3 lpm flow rate for different combination hybrid nanofluids. It can be seen from Fig. 4.42(a) that pressure drop is increasing with a decrease in aspect ratio. It has maximum value for aspect ratio of 2.5 for all the hybrid nanofluids. As the aspect ratio reduced from 5 to 2.5, the pressure drop increases by 27.25% for Al_2O_3+PCM mixture dispersed hybrid nanofluid. It is due to the increase in friction between fluid layers when flow through the low aspect ratio channel. The friction factor has a reverse trend from pressure drop with the channel aspect ratio shown in Fig. 4.42(b). As the channel aspect ratio is reduced, the friction factor increases. Friction factor directly proportional to pressure drop and hydraulic diameter and inversely promotional to the square of fluid velocity. Here the fluid velocity is increasing with the reduction of channel aspect ratio. Thus, the friction factor decreases with a reduction in channel aspect ratio from 5 to 2.5.

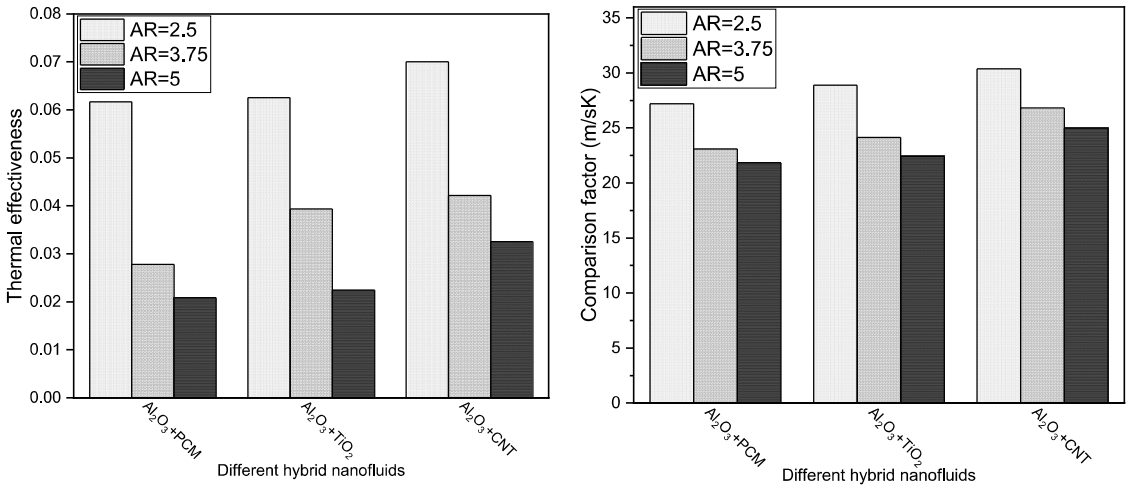

(a) (b)

Fig. 4.43 Effect of channel aspect ratio on (a) thermal effectiveness and (b) comparison factor

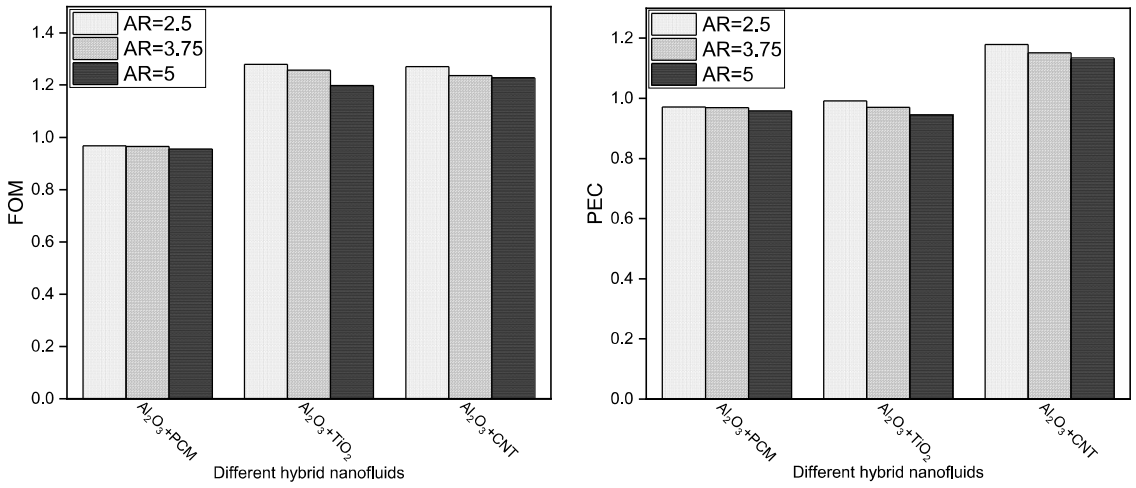

(a) (b)

Fig. 4.44 Effect of channel aspect ratio on (a) figure of merit and (b) performance evaluation criteria

The effect of channel aspect ratio on thermal effectiveness and comparison factor (heat transfer coefficient to the pressure drop ratio) is shown in Fig. 4.43(a) and 4.43(b), respectively. The thermal effectiveness of all the hybrid nanofluids decreases with a reduction in channel aspect ratio from 5 to 2.5, as shown in Fig. 4.43(a). This is because as the channel aspect ratio reduced, the fluid velocity increase leads to a reduction in temperature difference between the inlet and outlet of minichannel. The comparison factor increases when the aspect ratio of channel reduces from 5 to 2.5, as presented in Fig. 4.43(b) because the heat transfer coefficient increases at a faster rate compared to pressure drop with a reduction in channel aspect ratio. FOM and PEC values rise with a reduction in channel aspect ratio from 5 to 2.5, as depicts in Fig. 4.44(a) and 4.44(b), respectively. It can be supported by the fact that the heat transfer coefficient ratio increases at a faster rate as compared to the pressure drop ratio when the channel aspect ratio reduces from 5 to 2.5.

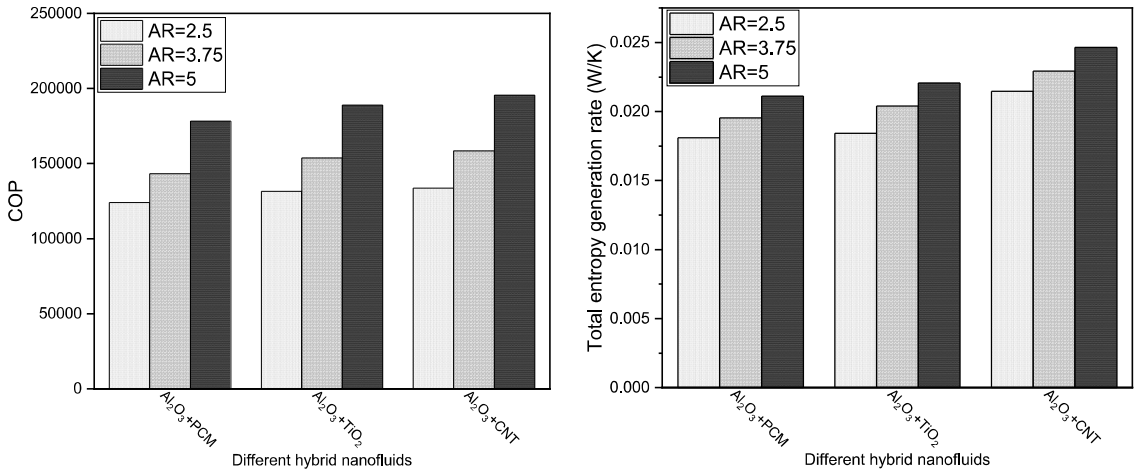

(a) (b)

Fig. 4.45 Effect of channel aspect ratio on (a) coefficient of performance and (b) total entropy generation rate

Fig. 4.45(a-b) depicts the effect of channel aspect ratio on the coefficient of performance and total entropy generation rate. It can be seen that the coefficient of performance decreases with a reduction in the channel aspect ratio, as shown in Fig. 4.45(a). As the channel aspect ratio decreases, the heat transfer reduces because of less temperature difference between the inlet and outlet of channel and pressure drop rise up due to an increase in wall shear stress and friction between fluid layers. It can be seen from Fig. 4.45(b) that the total entropy generation rate decreases when the channel aspect ratio reduces from 5 to 2.5. It can be concluded because friction entropy generation rises at a lower rate compared to increment in thermal entropy generation with a reduction in channel aspect ratio.

4.4.7 Composite particle dispersed hybrid nanofluid

In this section, the performance of minichannel heat sink is analyzed using rGO-ZnO composite dispersed hybrid nanofluid. This investigation is carried out at a nanoparticle volume concentration of 0.01% and a fluid inlet temperature of 30^{o}C. Here, the effects of flow rate, channel aspect ratio and heat flux on performance parameters are discussed. Three different aspect ratios as AR1=2.5, AR2=3.75, AR3=5 and three different heat fluxes Q1=33.33 W/cm^2, Q2=50 W/cm^2, Q3=66.67 W/cm^2 are considered. For a particular volumetric flow rate, as the aspect ratio decreases, the fluid velocity increases.

Fig. 4.46 presents the effect of channel aspect ratio and heat flux on the heat transfer coefficient. The effect of channel aspect ratio is shown at fixed heat flux (i.e., Q2) and the effect of heat flux is represented at a fixed channel aspect ratio (i.e., AR2). The maximum heat transfer coefficient is found of 5219.58 W/m^{2}K for a low aspect ratio (i.e., AR1). An enhancement of 20.62% and 15.8% is observed in the heat transfer coefficient when compared to base fluid (DI water) for the AR1 aspect ratio at a flow rate of 0.1 and 0.5 lpm, respectively. It can be seen from the figure that the heat transfer coefficient increases when the channel aspect ratio is reduced from 5 to 2.5 at a fixed heat flux. A maximum enhancement of 47.2% is obtained when the channel aspect ratio reduces from 5 to 2.5. It can also understand that the heat transfer coefficient rises with an increase in heat flux from Q1 to Q3 at a fixed channel aspect ratio. As heat flux rises from Q1 to Q3, the heat transfer coefficient increases by 17.41% % for composite hybrid nanofluid at the AR2 aspect ratio. The enhancement in heat transfer coefficient is observed by about 5.2% due to the rise in heat flux for base fluid (DI water).

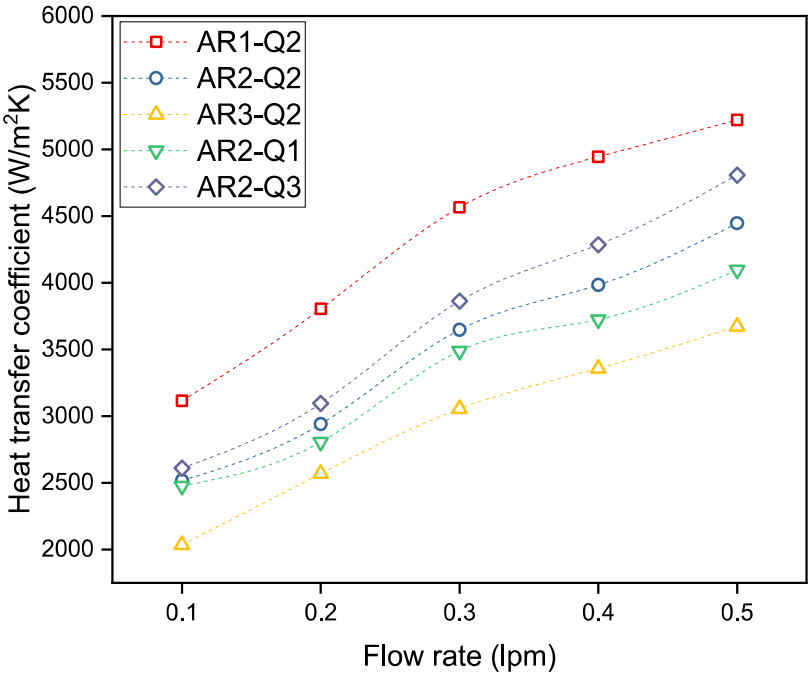

Fig. 4.46 Effect of channel aspect ratio and heat flux on heat transfer coefficient

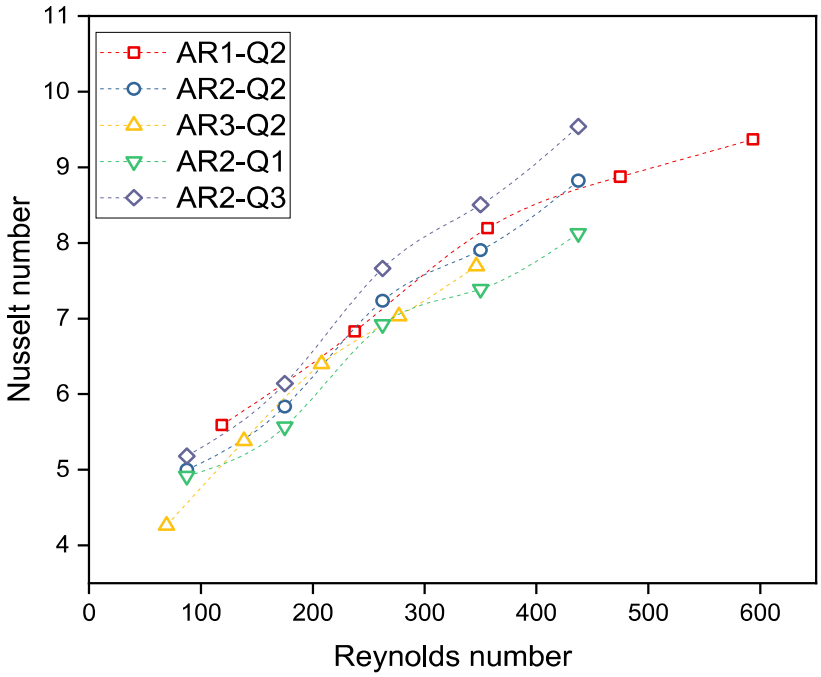

Fig. 4.47 Effect of channel aspect ratio and heat flux on Nusselt number

Nusselt number is maximum for channel 1 (AR1), having a maximum value of 9.37, as shown in Fig. 8. With an increase in Reynolds number, the Nusselt number is

continuing to increase. The effect of heat flux on the Nusselt number is the same as on the heat transfer coefficient. 17.36% enhancement is observed in Nusselt number when heat flux rises from Q1 to Q3. It is known that Nusselt number is directly proportional to heat flux This enhancement in Nusselt number is due to enhancement in heat flux is more as compared to enhancement in temperature difference between average surface temperature and mean temperature (i.e., T_s-T_m). Maximum Nusselt number enhancement of 16.7% is observed with composite nanofluid as compared to DI water.

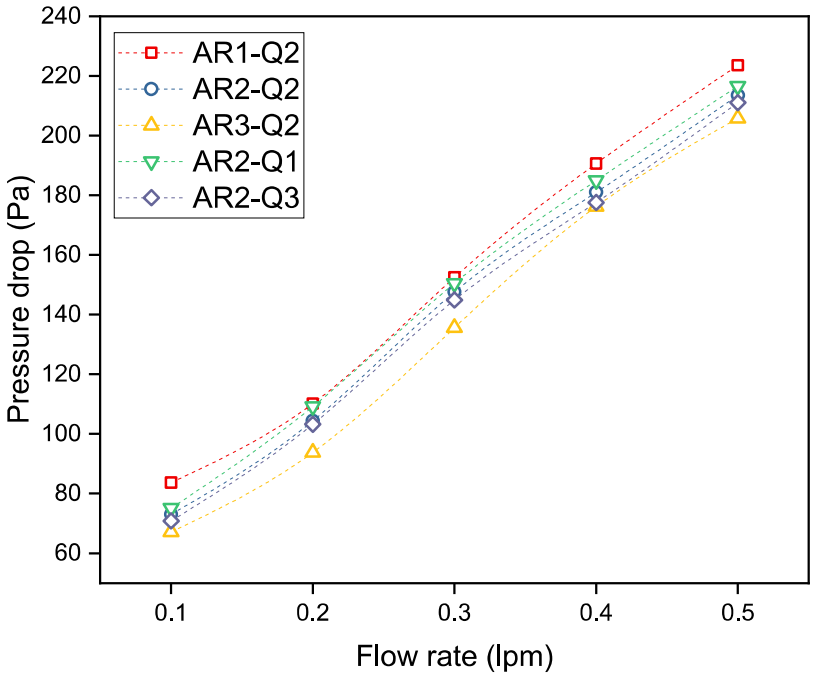

Fig. 4.48 Effect of channel aspect ratio and heat flux on pressure drop

Pressure drop is maximum for aspect ratio of AR1 and heat flux of Q2 because of the lower cross-section of the channel, as shown in Fig. 4.48. Pressure drop is continuously increasing with an increase in flow rate, as expected. As the channel aspect ratio decreases, the fluid velocity in the minichannel increases from 0.10 to 0.05 m/s at the flow rate of 0.1 lpm and from 0.52 to 0.26 at the flow rate of 0.5 lpm. Heat flux has a negative effect on the pressure drop. The maximum pressure drop is observed

as 334.2, 286.9 and 264.8 N/m^2 for composite hybrid nanofluid at the aspect ratio of AR1, AR2 and AR3, respectively, for fixed heat flux of Q1 (i.e., 33.33 W/cm^2). Pressure drop enhances about 5.04% when compared to DI water for AR1 and Q1 at 0.5 lpm. Heat sink having an AR3 aspect ratio shows the highest friction factor because of the lowest mean velocity. Minichannel wall shear stress increases with increased fluid velocity, resulting in a higher pressure drop. As the heat flux increases, the fluid viscosity reduces when flow through minichannel. This is the reason to fall in pressure drop correspond to heat flux. A significant effect of heat flux is observed at a lower flow rate (0.1 lpm), but at a higher flow rate, there is no significant effect is revealed. A reduction of 6.7% is found when heat flux increases from Q1 to Q3 at a 0.1 lpm flow rate.

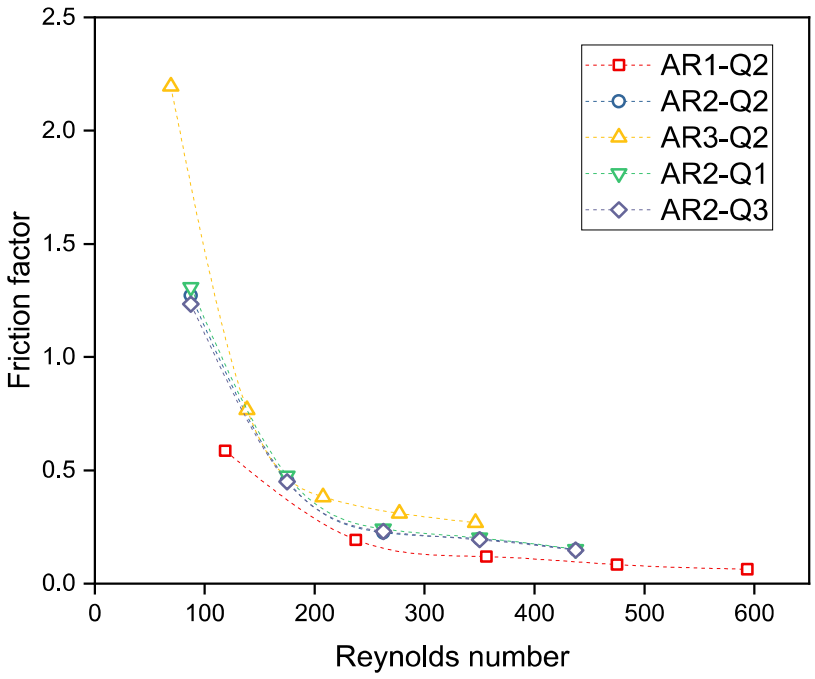

Fig. 4.49 Effect of channel aspect ratio and heat flux on friction factor

Fig. 4.49 depicts the variation of friction factor as a function of Reynolds number while changing the channel aspect ratio and heat flux. The friction factor is inversely

proportional to fluid velocity. It is predicted that a decrement in the friction factor observed with Reynolds number due to dual effects of (i) diminishing of boundary layer, and (ii) increase in mass velocity. The Friction factor has a significant deviation at lower Reynolds number, as shown in Fig. 4.49. This is because of that the wall shear stress rises drastically at lower Reynolds number and at high channel aspect ratio, fluid velocity decreases. Heat flux does not show any significant effect on friction factor throughout the range of Reynolds number. A maximum value of 2.2 is observed for a channel having an aspect ratio of AR3 at a constant heat flux of Q2.

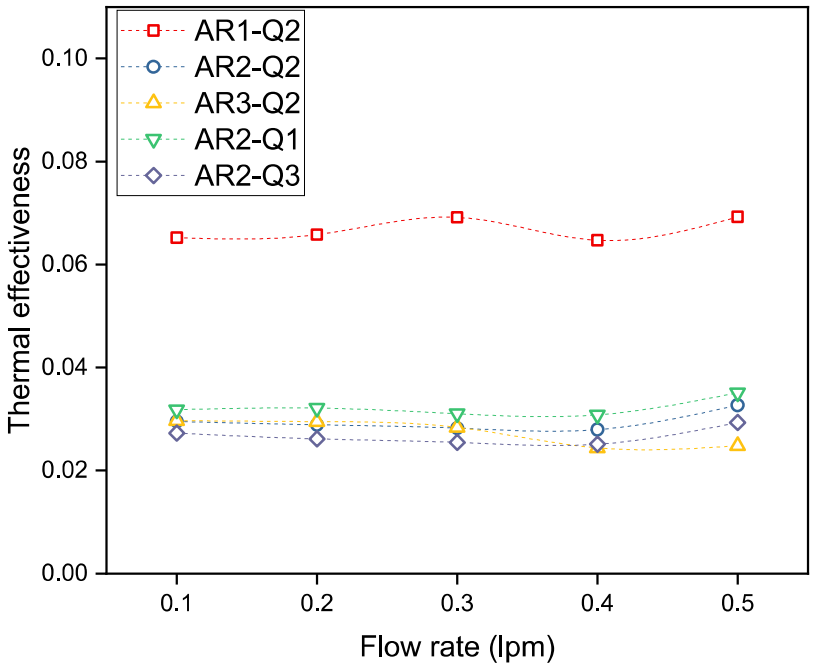

Fig. 4.50 Effect of channel aspect ratio and heat flux on thermal effectiveness

The thermal effectiveness of minichannel heat sink is presented in Fig. 4.50 as a function of flow rate (Reynolds number) at different channel aspect ratios and heat fluxes. Thermal effectiveness for the AR1 channel is maximum, as indicates in figure because it yields maximum heat transfer coefficient. Thermal effectiveness for AR1

(i.e., lower aspect ratio) channel is far away from other channels. This is because the temperature difference between the inlet and outlet of minichannel reduces as fluid velocity increases due to low cross-section at a constant volumetric flow rate. Thermal effectiveness reduces when heat flux increases from Q1 to Q3 due to a rise in temperature difference between the inlet and outlet of minichannel.

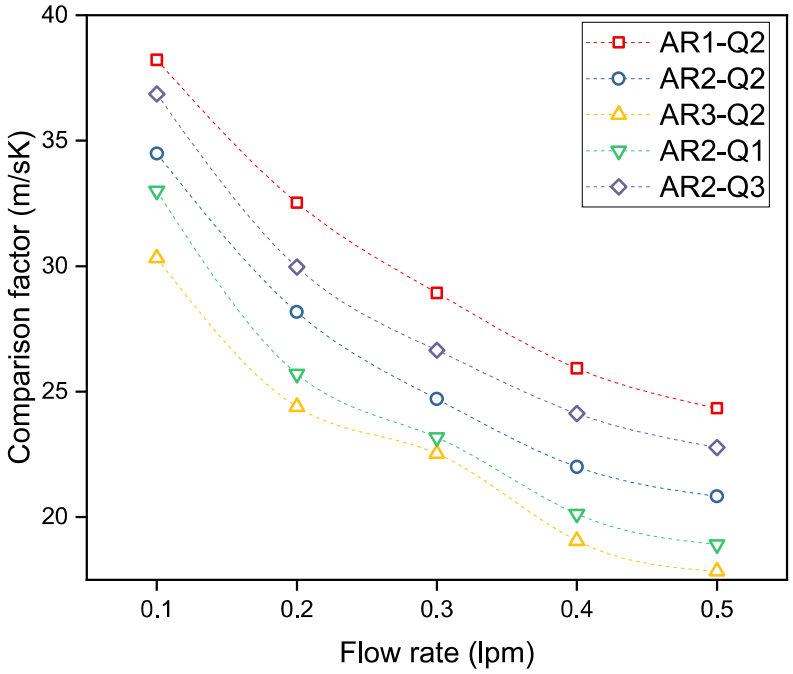

Fig. 4.51 Effect of channel aspect ratio and heat flux on comparison factor

The relative effect on the heat transfer coefficient and pressure drop is essential for practical applications. Fig. 4.51 depicts the comparison factor (heat transfer coefficient to pressure drop ratio, h/Δp) as a function of flow rate when variation in channel aspect ratio and heat flux. comparison factor decreasing as an impact of flow rate (Reynolds number) for all the combination of channel aspect ratio and heat flux. The maximum value of h/Δp ratio is for the channel aspect ratio of AR1 because of the heat transfer coefficient increases at a faster rate as compared to pressure drop. Heat flux has a positive impact on the heat transfer coefficient to the pressure drop ratio. As

heat flux rises, the h/Δp ratio is increasing because of an increase in heat transfer coefficient and a reduction in pressure drop.

The effect of channel aspect ratio and heat flux on the figure of merit as a function of flow rate is presented in Fig. 4.52. FOM has an optimum value at 0.4 lpm for all the combinations of channel aspect ratio and heat flux. As the aspect ratio decreases from 5 to 2.5, the FOM value rises. FOM has a maximum value of 1.39 for the AR2-Q3 combination at 0.4 lpm. For AR2-Q1 combination, FOM value at the lower flow rate is less than one, which is not desirable.

The variation of performance evaluation criteria (PEC) is shown in Fig. 4.53 as a function of flow rate for different combinations of heat flux and channel aspect ratio. It can be seen from the figure that PEC first falls up to 0.3 lpm and then it starts to rise up to 0.4 lpm and again starts to decreases. Thus, PEC has decreasing-increasing-decreasing trends with flow rate for all the combination of channel aspect ratio and heat flux. Both the heat flux and channel aspect ratio have a positive impact on PEC.

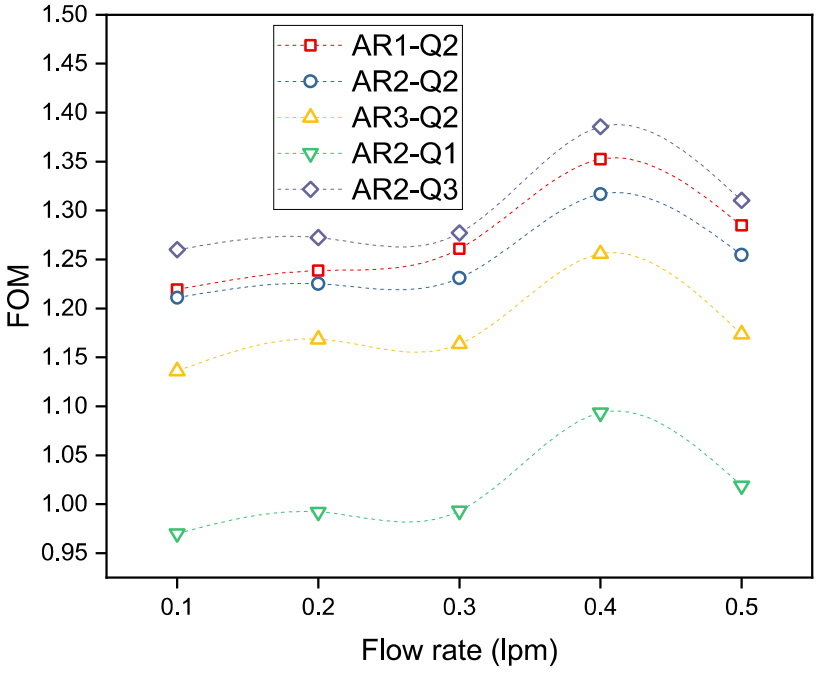

Fig. 4.52 Effect of channel aspect ratio and heat flux on figure of merit

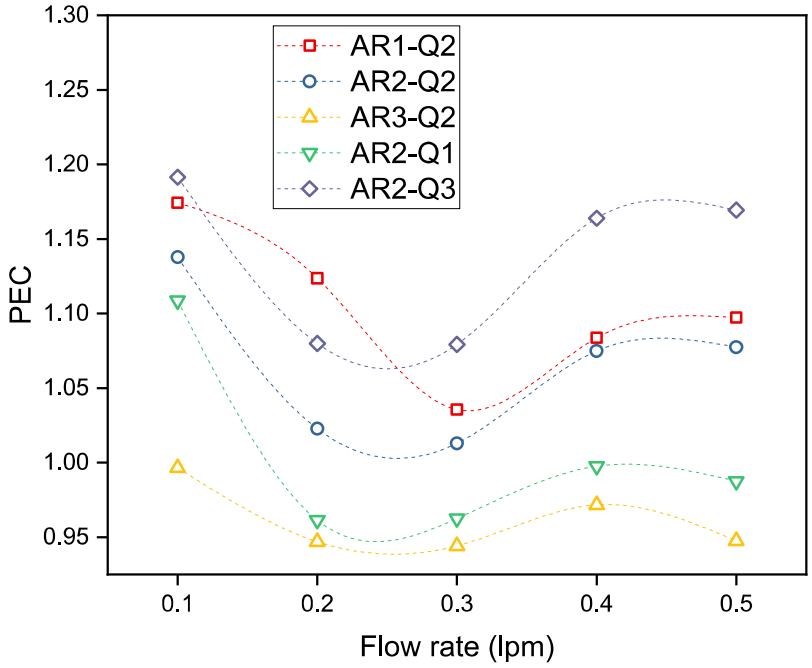

Fig. 4.53 Effect of channel aspect ratio and heat flux on performance evaluation criteria

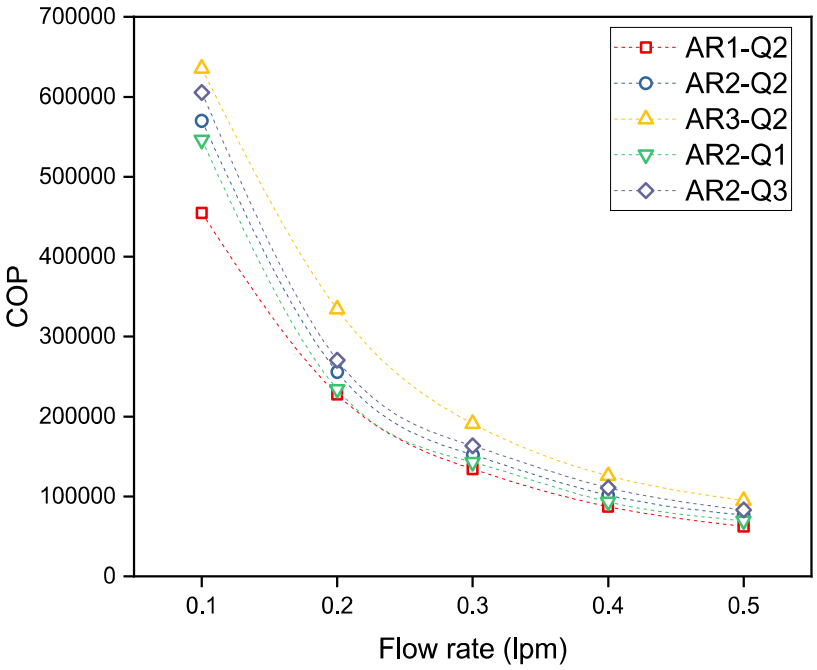

Fig. 4.54 Effect of channel aspect ratio and heat flux on coefficient of performance

The variation of coefficient of performance with flow rate is presented in Fig. 4.54 with different channel aspect ratios and heat fluxes. COP has decreasing

trends with flow rate. AR3-Q2 has the highest COP and AR1-Q2 has the lowest COP. As the heat flux increases, COP is increasing. As the channel aspect ratio decreases, the heat transfer increases due to a lower temperature differential between the inlet and outlet of the channel and the pressure drop rises due to increased wall shear stress and friction between the fluid layers as discussed above. COP is enhanced by 5.8 % when compared with that of base fluid (DI water) at a heat flux of Q2. The upper and lower limits for COP can not be decide because for different conditions (i.e., input heat flux and flow rate) it will vary. But in most of the cases, the COP lies between 10^3 to 10^7 for minichannel heat sink **(Ho et al., 2018 and 2019)**.

The effect of channel aspect ratio and heat flux on the total entropy generation rate at the range of flow rate from 0.1 lpm to 0.5 lpm is shown in Fig. 4.55. Total entropy generation rate increases with the flow rate. The total entropy generation rate decreases as the channel aspect ratio reduces from 5 to 2.5. AR3-Q2 has the highest total entropy generation rate and AR1-Q2 has the lowest total entropy generation rate.

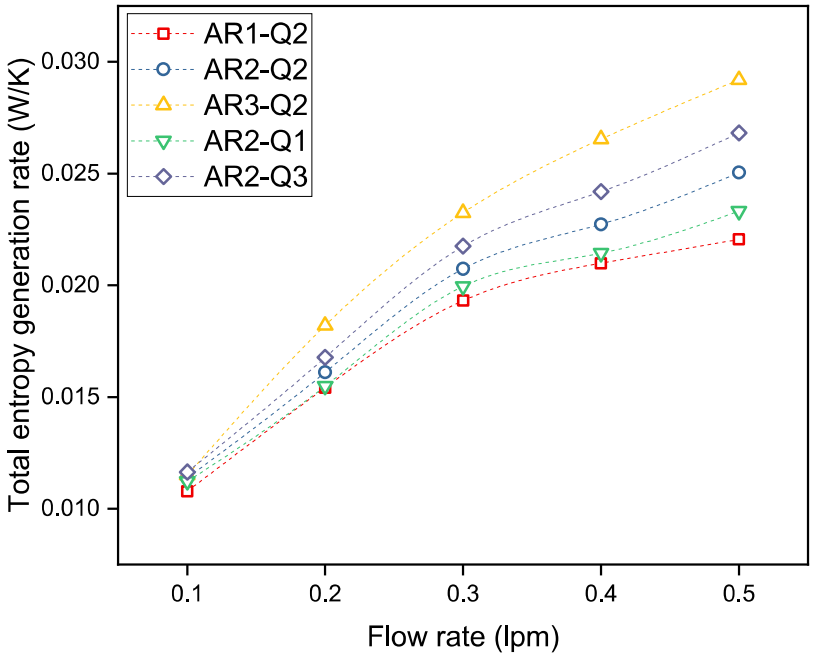

Fig. 4.55 Effect of channel aspect ratio and heat flux on total entropy generation rate

It can be inferred because the generation of friction entropy increases at a slower rate compared to the increase in thermal entropy generation with a decrease in the channel aspect ratio. The total entropy generation rate is enhanced by 31.2% and 18.6% for DI water and composite nanofluid with a reduction in aspect from AR1 to AR3 (i.e., 5 to 2.5) at a heat flux of Q2. Total entropy generation rate increases with the rise in heat flux. An enhancement of 15.02% has been observed in total entropy generation rate when heat flux rises from Q1 to Q3 (i.e., 33.33 to 66.67 W/cm^2) for composite hybrid nanofluid.

4.5 Highlights

- The increase in flow rate, nanoparticles dispersion in base fluid and increase in fluid inlet temperature have a positive impact on convective heat transfer coefficient and Nusselt number. Maximum enhancement is found for Al_2O_3+graphene dispersed hybrid nanofluid.
- The penalty of pressure drop is observed for all hybrid nanofluids. Fluid inlet temperature has a negative consequence on pressure drop. Reynolds number has an adverse effect on the friction factor.
- Thermal effectiveness has increasing, decreasing and again increasing trends with flow rate, although high conductivity particles dispersed nanofluids show high thermal effectiveness.
- Al_2O_3+AlN based hybrid nanofluid has a maximum comparison factor ($h/\Delta p$ ratio) and COP compared to all others working fluids in the range of flow rate from 0.1 lpm to 0.5 lpm.
- Al_2O_3+TiO_2 and Al_2O_3+CuO dispersed hybrid nanofluids is not a better candidate because of having low FOM and PEC.

- Both the heat transfer coefficient and pressure drop increase with a rise in nanoparticle volume concentration; however, no significant effect of their ratio (i.e., h/Δp) has been observed.
- The particle combination of dissimilar types (i.e., spherical-cylindrical) shows an optimum particle ratio of 3:2 for best hydrothermal performance in minichannel heat sink. However, no optimum ratio has been found for the particle combination of similar types (i.e., spherical-spherical).
- The heat transfer coefficient increases while pressure drop decreases with a rise in heat flux. Thus, a significant effect is observed on their ratio (i.e., comparison factor).
- Dispersion of Composite (rGO-ZnO) in base fluid (DI water) has a maximum heat transfer coefficient and pressure drop both for low aspect ratio (AR=2.75). Heat transfer coefficient increases and pressure drop decreases with an increase in the heat flux.
- The heat transfer coefficient and pressure drop both increase with a reduction in channel aspect ratio for a particular flow rate. But the combined effect is that the comparison factor increases with a decrease in channel aspect ratio. COP and total entropy generation rate decreases with a decrease in channel aspect ratio.
- Composite dispersed hybrid nanofluid yields better performance improvement even with lower volume concentration as compared to mixture dispersed hybrid nanofluid.